THESIS FOR THE DEGREE OF DOCTOR OF PHILOSOPHY IN SOLID AND STRUCTURAL MECHANICS

Finite element procedures for crack path prediction in multi-axial fatigue

DIMOSTHENIS FLOROS

Department of Industrial and Materials Science
CHALMERS UNIVERSITY OF TECHNOLOGY

Gothenburg, Sweden 2018

Finite element procedures for crack path prediction in multi-axial fatigue
DIMOSTHENIS FLOROS
ISBN 978-91-7597-849-9

Doktorsavhandlingar vid Chalmers tekniska högskola
Ny serie nr. 4530
ISSN 0346-718X
Department of Industrial and Materials Science
Chalmers University of Technology
SE-412 96 Gothenburg
Sweden
Telephone: +46 (0)31-772 1000

Cover:
Setting of twin-disc fatigue crack growth experiment (left), modeling of crack on the rail disc surface (upper right) and evaluation of crack growth direction from the maximum tangential stress range criterion (lower right).

Chalmers Reproservice
Gothenburg, Sweden 2018

Finite element procedures for crack path prediction in multi-axial fatigue
Thesis for the degree of Doctor of Philosophy in Solid and Structural Mechanics
DIMOSTHENIS FLOROS
Department of Industrial and Materials Science
Chalmers University of Technology

Abstract

Rolling Contact Fatigue (RCF) cracks in rails are among the most detrimental railway track defects regarding reliability and cost. The cracks typically grow in shear mode up to a certain length at which they might arrest or kink into a more tensile-driven growth. This growth scheme appears as a result of non-proportional loading, large plastic deformations at the rail surface and primary compression with crack-face friction. In contrast, most existing crack growth criteria in the literature feature quantities that are susceptible to the limitations of small-scale yielding, e.g. Stress Intensity Factors (SIFs), tensile-mode growth and unloaded crack-faces. Consequently, the range of validity of the existing criteria may be questioned in the non-linear crack growth setting of RCF.

In a study of the role of inelastic deformation on the crack loading, elastic–plastic simulations are carried out in pre-cracked tubular specimens subjected to mixed-mode cyclic loading. The crack loading is quantified via the Crack-Tip Displacements (CTDs) in modes I and II. Shakedown and ratcheting effects in the ranges of the CTDs are compared to trends of crack growth curves from experiments in the literature. It is concluded that the ranges of the CTDs can be used for qualitative crack growth assessment in the examined load cases. In addition, a gradient-enhanced mixed variational formulation is developed for overcoming the numerical difficulties associated with the computation of Configurational Forces (CFs) for inelasticity. The mesh sensitivity of the CFs acting on an embedded discrete singularity is investigated. Results highlight that the proposed formulation provides sufficient regularity for the computation of CFs, which may then be used in the formulation of criteria for RCF crack propagation.

Predictions of the multi-axial fatigue crack path are performed based on instantaneous crack growth direction criteria. To this end, a generic model for load cycle evaluation is proposed and implemented on criteria based on CFs and CTDs. The predicted directions are compared towards mixed-mode fatigue crack growth experiments from the literature. Of the evaluated criteria, the ones based on CFs and CTDs accurately predict the tensile-mode growth. Classical SIF-based criteria seem to handle tensile-mode growth under moderate shear-mode loading. Moreover, the criterion based on CTDs captures the shear-mode growth and the tensile-mode growth as well as the transition between them. The latter growth schemes essentially resemble the RCF crack growth.

In an investigation of the influence of various railway operational parameters on predicted RCF crack growth directions, the coefficient of friction at the wheel–rail interface was found the most influential as compared to the wheel tonnage and crack-face friction. The latter had no effect on predicted directions, due to crack-tip opening at the instances of maximum shear CTDs.

Keywords: Numerical simulation, Mixed-mode, Fracture mechanics, Configurational forces, Rolling contact fatigue, Plasticity.

To my parents, Theodoros and Giannoula Floros

Preface

The work in this thesis is part of CHARMEC center of excellence in railway mechanics, Department of Industrial and Materials Science, Chalmers University of Technology, Gothenburg, Sweden. The research performed within the project was supported financially and in-kind by Trafikverket and voestalpine Schienen, for which they are gratefully acknowledged. Part of the research was funded by the European Union's Horizon 2020 research and innovation program in the project In2Track2 under grant agreement No 730841.

Few people have contributed to this work and I hereby thank them for this. First, I would like to acknowledge Professor Kenneth Runesson primarily for his theoretical work that part of the thesis has stepped on and moreover for being a model for excellence at research in mechanics. Next, I would like to express my gratitude to my main supervisors, Professor Fredrik Larsson and Professor Anders Ekberg. The former, with his knowledge and ideas, has helped me realize how fascinating the combination of continuum and computational mechanics can be. The latter has been generously sharing his expertise in railway mechanics as well as in engineering solution finding. Thank to all three of you for your support and the numerous very fruitful meetings. Furthermore, I would like to thank my colleagues at the Division of Material and Computational Mechanics as well as at the Division of Dynamics at Chalmers University of Technology for contributing to a very joyful working environment.

Finally, I owe gratitude to my parents, Theodoros and Giannoula Floros for always being there for me as model parents they are! Special thanks goes also to my uncle, Major General Dimosthenis Floros for his generous support throughout my studies. Last but not least, I am thankful to my girlfriend Gelena Andreasian for her patience, understanding and help during the last two and a half years.

Gothenburg, 2018
Dimosthenis Floros

Thesis

This thesis consists of an extended summary and the following appended papers:

Paper A D. Floros, A. Ekberg, and K. Runesson. A numerical investigation of elastoplastic deformation of cracks in tubular specimens subjected to combined torsional and axial loading. *International Journal of Fatigue* **91** (2016), 171–182. DOI: 10.1016/j.ijfatigue.2016.06.008

Paper B D. Floros, F. Larsson, and K. Runesson. On configurational forces for gradient-enhanced inelasticity. *Computational Mechanics* **61**.4 (2018), 409–432. DOI: 10.1007/s00466-017-1460-x

Paper C D. Floros, A. Ekberg, and F. Larsson. Evaluation of crack growth direction criteria on mixed-mode fatigue crack growth experiments. *Submitted for international publication* (2018)

Paper D D. Floros, A. Ekberg, and F. Larsson. "Evaluation of mixed-mode crack growth criteria under rolling contact conditions". *Proceedings of the 11th International Conference on Contact Mechanics and Wear of Rail/Wheel Systems*. TU Delft, 2018, pp. 253–260

Paper E D. Floros, A. Ekberg, and F. Larsson. Evaluation of rolling contact fatigue crack growth directions in rails under varying operational conditions. *To be submitted for international publication* (2018)

The appended papers have been prepared in collaboration with the co-authors. The author of this thesis was the main responsible for the progress of the work. Namely, took part in planning of the papers and the development of the theory, carried out numerical implementation and simulations, and wrote major parts of the papers.

Contents

Part I
Extended Summary

1 Introduction

1.1 Motivation for research and background

Among railway track surface defects, *head checks* are considered one of the most detrimental in terms of reliability and cost. These are small, parallel cracks, inclined to the running direction, that appear at the gauge corner of the high rail in curves, see Fig 1.1. Head checks are rolling contact fatigue (RCF) phenomena. RCF cracks stem from internal or surface defects in the rail material that tend to propagate under the action of the (frictional) rolling contact due to the passage of wheels. The severity of the load situation may be better viewed considering that the wheel–rail contact patch is similar in size to that of a small coin, see Marshall et al. [6]. The maximum static axle load which is carried on two such surfaces is to-date as high as 30 t, with extreme cases up to and above 42 t, see Girsch et al. [7].

Figure 1.1: *RCF cracks and spalls near the gauge corner of a rail.*

Regarding growth of head checks with time, there are two prominent scenarios: After an initial stage of growth in a shallow inclination from the rail surface, the RCF cracks grow upwards causing spalling of the railway material. Alternatively, they grow downwards, transversely towards the longitudinal axis of the rail, finally resulting in complete failure of the rail. Both scenarios induce reliability issues to the railway operation. They also lead to environmental effects and high maintenance costs, see Magel [8]. To prevent and mitigate these issues, the need for *accurate prediction of the direction and the rate of*

RCF crack propagation is vital.

Surface crack growth of the kind that appears in rails is a complex phenomenon which is neither fully understood nor captured by the predictive criteria that are currently available in the literature. Rolling contact conditions typically result in non-proportional load cycles. Furthermore, the passage of the wheel–rail contact patch over the RCF cracks induces primary compression to the crack-faces. This magnifies the effect of crack-face friction on crack growth. The fatigue situation is further complicated by the (large) plastic deformations at the surface of the rails and the near-tip regions of the RCF cracks. These factors of complexity are dealt with in the current thesis, but it is, by far, a non-exhaustive list. Other factors that contribute to a convoluted RCF situation are the anisotropy of the severely deformed contact surfaces of the rails and wheels (Larijani et al. [9]), the wear of wheel and rail materials which acts in competition to the rate of RCF crack growth (Brouzoulis [10]) and the effect of lubrication that may penetrate the RCF cracks (Bower [11]).

In contrast to the high demands set on fatigue crack growth criteria by the RCF crack growth setting, the existing methods for prediction of the crack growth direction and rate of RCF cracks are susceptible to limitations. The crack loading in the majority of the existing RCF crack growth criteria is quantified using Stress Intensity Factors (SIFs). These are, in theory, limited to small-scale plasticity which contradicts with the gross plasticity present in RCF of rails and wheels, see Ringsberg [12]. In addition, the non-proportional rolling contact load cycles urge for an appropriate method to perform load cycle evaluation. This is most often performed in the literature by determination of the range of SIFs over the evaluated wheel passage. In the general crack growth setting though, it is not always clear how to define a load cycle. In addition, the entire range may not be fully applicable on the crack and definition of effective ranges of SIFs becomes a necessity, see Wong et al. [13].

In this regard, the thesis aims to contribute towards addressing some of the fundamental issues that criteria for RCF crack growth prediction need to handle. This includes, to contribute to the evaluation of existing, and derivation of alternative crack-driving force parameters, that are not bound to limitations pertinent to quantities such as the SIFs. The best performing existing and derived parameters may then be used in the formulation of crack propagation criteria. Furthermore, elaborating on the way to perform load cycle evaluation is another goal of the thesis. For this purpose, a generic model for load cycle evaluation is proposed. The proposed model and currently employed methods for load cycle evaluation are implemented here in a thorough investigation of mixed-mode crack growth direction criteria and comparison towards a multitude of experiments from the literature. Advances in RCF crack growth predictive methods are expected to contribute to optimization of the maintenance process of railway tracks in terms of more targeted inspection intervals, reduced disturbance of traffic for maintenance work and more efficient use of resources. This is achieved through avoiding premature replacement/removal of railway steel material, through grinding/turning, or through replacement.

1.2 Purpose and outline of the thesis

In Chapters 2 and 3, the two core issues that the thesis deals with are investigated; the derivation and identification of appropriate ***quantities for quantification of the mixed-mode crack loading for inelasticity*** are performed in Chapter 2. A state-of-the-art review of candidate quantities in the literature is performed in Section 2.1. In Section 2.2, a remedy is proposed to overcome numerical difficulties associated with the computation of configurational forces for inelasticity (paper B [2]). In Section 2.3, the potential of crack-tip displacements as parameters for the qualitative assessment of crack growth is examined (paper A [1]). Conclusions from the study of quantities for measuring the crack loading are drawn in Section 2.4.

In Chapter 3, existing and new ***numerical procedures for crack path prediction in multi-axial fatigue*** are investigated. Conclusions from a survey of existing criteria for prediction of the multi-axial fatigue crack path are summarized in Section 3.1. In Section 3.2, instantaneous mixed-mode crack growth direction criteria from the literature are briefly described and a framework for their evaluation is proposed (paper C [3]). Application of the framework is illustrated on simulations of tensile- and shear-mode fatigue crack growth experiments from the literature in Section 3.3 (papers C [3] and D [4]). The effect of various railway operational parameters on RCF crack growth direction predictions is overviewed in Section 3.4 (paper E [5]). Conclusions from the numerical procedures for multi-axial fatigue crack path prediction are outlined in Section 3.5.

A list of software that were used for the computations with special focus at an in-house finite element software is provided in Chapter 4. Summaries of the appended journal papers that contain the bulk of the material discussed in this thesis are provided in Chapter 5. Concluding remarks and future work stemming from the thesis are discussed in Chapter 6.

2 The effect of inelastic deformation on crack loading

2.1 State-of-the-art

Traditionally, crack loading is quantified by Stress Intensity Factors (SIFs). These are, at least in theory, susceptible to the limitations of: (a) small-scale yielding and (b) sufficiently long cracks compared to the material microstructure, see Dowling [14]. Thus, for short cracks embedded in severely deformed plastic layers (like incipient RCF cracks), SIFs are not suitable measures, see Ringsberg [12]. In the presence of large plastic deformations, a quantification using strain intensity factors improves the correlation with experimental crack growth rate curves, see Brown et al. [15].

Apart from the aforementioned limitations, fatigue crack growth evaluation is further complicated by the need to account for the evolution of the stress components during a load cycle. This is in the following termed "load cycle evaluation". Commonly in the literature the load cycle evaluation is accomplished by employing the range of the measured quantity over the load cycle. In case of mixed-mode loaded cracks, a plethora of equivalent ranges of SIFs has been proposed. These are, essentially, non-linear functions of the ranges of SIFs in the fatigue modes that are present, see Tanaka [16]. A review of equivalent ranges of SIFs is performed in Rozumek and Macha [17]. The equivalent ranges of SIFs are often used in Paris-type models for crack propagation. In turn, the material parameters of the Paris-type models and the unknown coefficients and/or exponents in the expressions of the equivalent ranges of SIFs that give the best fit to crack growth rates from experiments are identified. In this context, effects such as crack-closure and friction are modeled by e.g. scaling the nominal ranges of SIFs by factors such as the crack-closure ratio, see e.g. Wong et al. [13].

Measures of the crack loading that are not influenced by limitations pertinent to the material response are the Crack-Tip Opening Displacement (CTOD) and Crack-Tip Shear Displacement (CTSD), see e.g. Tschegg et al. [18]. For linear elastic bulk material response, the CTOD and CTSD become functions of the SIFs, see Li [19]. A complication with these measures is that there is no consensus on how far away from the crack-tip the displacements should be measured, especially under elastic–plastic conditions. Thus, the benefit of measuring the severity of the crack situation (in theory) at an infinitesimal distance from the crack-tip with the SIFs may be lost when using the CTOD and CTSD. Implementation of the ranges of CTOD and CTSD in a criterion for fatigue crack propagation is performed in Li [19]. A method to account for crack-closure effects on fatigue crack growth rate is proposed in Tschegg [20]. The method is based on extrapolation of the crack growth rate at a specified level of fatigue loading (measured in terms of the CTOD) to the theoretical rate at zero crack length, termed as "true" crack growth rate.

A scalar parameter frequently employed in fatigue analysis is the J-integral, see Rice [21]. In its classic form, the J-integral reflects the global energy release rate due to (virtual) unit crack advance in the crack-tip direction. The cyclic J-integral (also

known as the ΔJ-integral[1]) is used in Dowling and Begley [22] to describe fatigue crack growth accompanied by gross plasticity. In Tanaka [23], a physical interpretation of the ΔJ-integral is offered and its path-dependence is discussed for linear elastic and elastic–plastic material response. In overall, it may be argued that path-independence of the ΔJ-integral is limited to stabilized cyclic material response and more specifically to total deformation theory of plasticity, similarly to the classic J-integral, see Wüthrich [24]. For mixed-mode loaded cracks, it is possible to determine the SIFs in the modes that are present from decomposition of the J-integral into the pertinent modes, see e.g. Alfredsson and Olsson [25]. To account for non-proportional loading, elastic–plastic material response and crack-closure, an effective ΔJ-integral is proposed in Döring et al. [26]. The effective ΔJ-integral resulted in satisfying accuracy of predicted fatigue lives as compared to experiments. In Hoshide and Socie [27], it is postulated that the fatigue crack growth rate under mixed-mode conditions may be expressed as a linear combination of the rates in the modes that are present. In turn, the rates in pure modes I and II can be expressed in terms of the ΔJ-integral for a certain class of materials via the HRR crack-tip fields (Hutchinson [28]). Good correlations to fatigue crack growth rates from experiments in terms of the ΔJ-integral have been demonstrated among other sources in Dowling and Begley [22], Chen and Keer [29] and Hos and Vormwald [30].

The concept of configurational (or material) forces has also been employed in fracture and fatigue analyses. Configurational forces are fictitious forces related to the global energy release rate in a continuum that undergoes spatial and configurational motion, such as a crack advance, see Tillberg et al. [31]. In the linear elastic case, the J-integral is retrieved by projection of the configurational force onto the undeformed crack-tip direction. However, the configurational force is a vectorial quantity, and as such, carries more information than the scalar J-integral, see Steinmann [32]. The use of configurational forces therefore provides a rather generic framework to account for the energy release rate related to both the crack advance and material dissipation. The energy release rate computed from configurational forces retains path-independence in a similar way as the classic J-integral, see Näser et al. [33]. Despite the path-independence, the computed energy release rate exhibits pathological FE-mesh sensitivity in the inelastic regime[2], see Tillberg et al. [31]. The sensitivity is attributed to discretization errors related to the differentiation of the steep plastic gradients in the near-tip region that emerges in the expression for the configurational force, see paper B [2].

The discussion in this section reiterated some of the issues related to the quantification of mixed-mode crack loading that are currently not fully addressed in the literature.

1. **The cyclic elastic–plastic material response imposes limitations on most quantities used to quantify the crack loading**.

   The limits on the applicability of Linear Elastic Fracture Mechanics (LEFM) have led to the proposal and investigation of alternative quantities to measure the intensity of

[1]The symbol "Δ" should not be confused here with the range operator, i.e. $\Delta J \neq J_{\max} - J_{\min}$. It is used in the literature to denote the change of the J-integral during the load cycle from a reference "unloaded" state to the state of "maximum loading".

[2]As regards projection of the configurational force onto the transverse to the undeformed crack-tip direction, it is shown in Brouzoulis and Ekh [34] that the pertinent scalar quantity is path-dependent even in the (hyper-)elastic case.

the crack situation in the presence of inelastic deformations, such as the J-integral and the CTOD and CTSD. The pertinent quantities are typically categorized under the realm of Elastic–Plastic Fracture Mechanics (EPFM). The mesh sensitivity of the energy release rates computed from configurational forces for inelasticity is investigated in Section 2.2 and paper B [2]. The appropriateness of the CTOD and CTSD as EPFM quantities to measure the crack loading is qualitatively examined in Section 2.3 and paper A [1].

2. **There is no consensus on how to account for non-proportional loading in the quantification of mixed-mode crack loading**.

   The way to perform load cycle evaluation and the lack of a generally applicable quantity to quantify the mixed-mode fatigue crack growth still comprise open topics for investigation in the general inelastic fatigue crack growth setting, see Zerres and Vormwald [35]. Investigations of how to perform load cycle evaluations are discussed in Chapter 3 and papers C [3] and D [4].

2.2 Configurational forces based on a gradient-enhanced mixed formulation

In [31] and [33], it is shown that the computation of configurational forces for (local) inelasticity is sensitive to the chosen FE-mesh size in problems involving discrete singularities. Two of the reasons that have been identified as causes for this sensitivity are:

(a) The discretization error arising from nodal smoothing techniques in the computation of the spatial gradient of the internal variables in displacement-based variational formulations. In such formulations, values of the internal variables are known only at the integration points, thereby nodal smoothing is required during post-processing for the subsequent evaluation of the spatial gradient of the internal variables.

(b) The steep gradient fields in the vicinity of the crack-tip that cannot be adequately resolved by the derivatives of standard (polynomial) shape functions.

To this end, the primary aim in paper B [2] is to derive a crack-driving force parameter for inelasticity based on configurational forces that is computable with mesh-refinement. This is attempted by two synergistic measures:

(a) Gradient effects are taken into account in the constitutive setting, thus contributing in regularization of the steep gradients mentioned above.

(b) A mixed variational formulation is constructed in terms of the displacements and a gradient field, the latter being the stress measure which is energy-conjugated to the spatial gradient of the internal variables. This, provides a continuous approximation of the gradient field after numerical solution of the proposed mixed variational formulation. Thereby, no heuristic post-processing is required for the computation of the gradient field.

2.2.1 Spatial motion problem

The gradient-enhanced mixed variational formulation is for illustrative purposes derived here for perfect viscoplasticity of Bingham type. The model is enhanced by a gradient term, such that the free energy may be written as

$$\psi(\boldsymbol{\epsilon}, \boldsymbol{\epsilon}^{\mathrm{p}}, \boldsymbol{g}) = \underbrace{\frac{1}{2}[\boldsymbol{\epsilon} - \boldsymbol{\epsilon}^{\mathrm{p}}] : \mathbf{E}^{\mathrm{e}} : [\boldsymbol{\epsilon} - \boldsymbol{\epsilon}^{\mathrm{p}}]}_{\psi^{\mathrm{loc}}(\boldsymbol{\epsilon}, \boldsymbol{\epsilon}^{\mathrm{p}})} + \underbrace{\frac{1}{2} H_{\mathrm{g}} l_{\mathrm{s}}^2 |\boldsymbol{g}|^2}_{\psi^{\mathrm{gra}}(\boldsymbol{g})}, \tag{2.1}$$

where $\mathbf{E}^{\mathrm{e}}$ is the elastic stiffness tensor, $\boldsymbol{\epsilon}(\boldsymbol{x}, t) = [\boldsymbol{u} \otimes \boldsymbol{\nabla}]^{\mathrm{sym}}$ is the engineering strain, $\boldsymbol{\epsilon}^{\mathrm{p}}(\boldsymbol{x}, t)$ is the plastic strain, H_{g} is the gradient hardening modulus and $\boldsymbol{g}(\boldsymbol{x}, t) \overset{\mathrm{def}}{=} \boldsymbol{\epsilon}^{\mathrm{p}} \otimes \boldsymbol{\nabla}$. Square brackets $[\diamond]$ denote operational dependence of the argument. The gradient term in Eq. (2.1) is scaled by an internal length, l_{s}. The latter may be viewed as a regularization parameter, i.e. $l_{\mathrm{s}} = 0$ corresponds to the classical local model. In addition, a (dual) dissipation potential ϕ^* in terms of the dissipative stress, $\boldsymbol{\kappa}^{\mathrm{di}}$, is assumed. From Eq. (2.1), the following energetic variables are defined,

$$\boldsymbol{\sigma} \overset{\mathrm{def}}{=} \frac{\partial \psi}{\partial \boldsymbol{\epsilon}}, \quad \boldsymbol{\xi} \overset{\mathrm{def}}{=} \frac{\partial \psi}{\partial \boldsymbol{g}}. \tag{2.2}$$

In order to arrive to FE-equations whose linearization yields a symmetric stiffness matrix (see also Remark 3 in paper B [2]), we derive a *semi-dual* free energy that depends on $\boldsymbol{\xi}$ rather than on $\boldsymbol{g}$. This is accomplished by an appropriate Legendre transformation, which allows for stating the semi-dual free energy of the gradient-enhanced viscoplastic model as

$$\varphi(\boldsymbol{\epsilon}, \boldsymbol{\epsilon}^{\mathrm{p}}, \boldsymbol{\xi}) = \underbrace{\frac{1}{2}[\boldsymbol{\epsilon} - \boldsymbol{\epsilon}^{\mathrm{p}}] : \mathbf{E}^{\mathrm{e}} : [\boldsymbol{\epsilon} - \boldsymbol{\epsilon}^{\mathrm{p}}]}_{\psi^{\mathrm{loc}}(\boldsymbol{\epsilon}, \boldsymbol{\epsilon}^{\mathrm{p}})} - \underbrace{\frac{1}{2 H_{\mathrm{g}} l_{\mathrm{s}}^2} |\boldsymbol{\xi}|^2}_{\psi^{*,\mathrm{gra}}(\boldsymbol{\xi})}. \tag{2.3}$$

Thereby, the constitutive equation for $\boldsymbol{g}(\boldsymbol{\xi})$ is derived from Eq. (2.3),

$$\boldsymbol{g}(\boldsymbol{\xi}) = -\frac{\partial \varphi}{\partial \boldsymbol{\xi}}. \tag{2.4}$$

Taking Eq. (2.4) into account, the balance equations of the proposed mixed-*dual* format are obtained as: Find $\boldsymbol{u}(\boldsymbol{x})$, $\boldsymbol{\xi}(\boldsymbol{x})$, $\boldsymbol{\epsilon}^{\mathrm{p}}(\boldsymbol{x})$ and $\boldsymbol{\kappa}^{\mathrm{di}}(\boldsymbol{x})$ that satisfy

$$-\boldsymbol{\sigma}(\boldsymbol{\epsilon}[\boldsymbol{u}], \boldsymbol{\epsilon}^{\mathrm{p}}) \cdot \boldsymbol{\nabla} = \mathbf{0} \text{ in } \Omega \times \mathbb{R}^+, \tag{2.5}$$

$$-\boldsymbol{\sigma}(\boldsymbol{\epsilon}[\boldsymbol{u}], \boldsymbol{\epsilon}^{\mathrm{p}}) + \boldsymbol{\kappa}^{\mathrm{di}} - \boldsymbol{\xi} \cdot \boldsymbol{\nabla} = \mathbf{0} \text{ in } \Omega \times \mathbb{R}^+, \tag{2.6}$$

$$\boldsymbol{g}[\boldsymbol{\epsilon}^{\mathrm{p}}] - \boldsymbol{g}(\boldsymbol{\xi}) = \mathbf{0} \text{ in } \Omega \times \mathbb{R}^+, \tag{2.7}$$

$$\dot{\boldsymbol{\epsilon}}^{\mathrm{p}} - \frac{\partial \phi^*}{\partial \boldsymbol{\kappa}^{\mathrm{di}}}(\boldsymbol{\kappa}^{\mathrm{di}}) = \mathbf{0} \text{ in } \Omega \times \mathbb{R}^+, \tag{2.8}$$

as well as the boundary conditions (see Fig. 2.1),

$$\boldsymbol{u} = \boldsymbol{u}_{\mathrm{p}} \text{ on } \partial\Omega_{\mathrm{u}}, \ \boldsymbol{t} = \boldsymbol{t}_{\mathrm{p}} \text{ on } \partial\Omega_{\mathrm{t}}, \tag{2.9}$$

$$\boldsymbol{p} = \boldsymbol{p}_{\mathrm{p}} \text{ on } \partial\Omega_{\mathrm{p}}, \ \boldsymbol{\epsilon}^{\mathrm{p}} = \boldsymbol{\epsilon}^{\mathrm{p}}_{\mathrm{p}} \text{ on } \partial\Omega_{\mathrm{k}}. \tag{2.10}$$

Equation (2.5) is the standard equilibrium under quasi-static conditions (in the absence of volume forces), while Eq. (2.6) is termed the "micro-force" balance equation in e.g. [36]. Coupling between all the primary fields becomes evident from the latter equation. Furthermore, the standard Dirichlet and Neumann boundary conditions on $\boldsymbol{u}$ and $\boldsymbol{t}$ are set in Eq. (2.9). In Eq. (2.10), the rather non-standard boundary conditions appear on micro-traction, $\boldsymbol{p} \stackrel{\text{def}}{=} \boldsymbol{\xi} \cdot \boldsymbol{n}$, and $\boldsymbol{\epsilon}^{\text{p}}$. In paper B [2], the "extreme" choices of "free" ($\boldsymbol{p} = \boldsymbol{0}$) and "hard" ($\boldsymbol{\epsilon}^{\text{p}} = \boldsymbol{0}$) boundary conditions are considered.

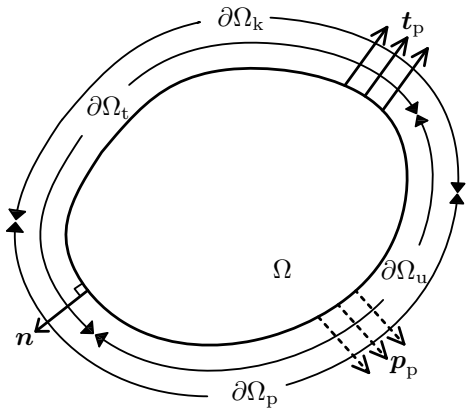

Figure 2.1: *Body occupying the domain Ω, surface tractions $\boldsymbol{t}_{\text{p}}$, micro-tractions $\boldsymbol{p}_{\text{p}}$ and normal $\boldsymbol{n}$. Dual partitioning of the boundary is introduced as $\partial\Omega = \partial\Omega_{\text{u}} \cup \partial\Omega_{\text{t}} = \partial\Omega_{\text{p}} \cup \partial\Omega_{\text{k}}$.*

Applying the principle of virtual work and Green-Gauss theorem (where appropriate), the mixed-dual variational format is obtained. For clarity, this is written below in terms of global and local sets of equations. The global equations are stated in Eqs. (2.11) and (2.12). As for the variational form of Eqs. (2.6) and (2.8), no gradient of the pertinent test functions appears in the variational format, thereby these equations can be satisfied in a strong sense. In addition, elimination of $\boldsymbol{\kappa}^{\text{di}}$ from the latter equations results in residual equation (2.13). All the fields appearing in the global/local structure, Eqs. (2.11)–(2.13), pertain to time-discrete fields, after application of the Backward-Euler time integration rule in the time interval, $(t_n, t_{n+1}]$.

Global: Find $\boldsymbol{u}(\boldsymbol{x})$ and $\boldsymbol{\xi}(\boldsymbol{x})$, such that:

$$R_u(\boldsymbol{u}, \boldsymbol{\xi}; \delta\boldsymbol{u}) \stackrel{\text{def}}{=} \int_\Omega \boldsymbol{\sigma}(\boldsymbol{\epsilon}[\boldsymbol{u}], \boldsymbol{\epsilon}^{\text{p}}\{\boldsymbol{\epsilon}[\boldsymbol{u}], \boldsymbol{\chi}[\boldsymbol{\xi}]\}) : \boldsymbol{\epsilon}[\delta\boldsymbol{u}] \, \text{d}\Omega - l^{(u)}(\delta\boldsymbol{u}) = 0, \tag{2.11}$$

$$R_\xi(\boldsymbol{u}, \boldsymbol{\xi}; \delta\boldsymbol{\xi}) \stackrel{\text{def}}{=} \int_\Omega [-\boldsymbol{\epsilon}^{\text{p}}\{\boldsymbol{\epsilon}[\boldsymbol{u}], \boldsymbol{\chi}[\boldsymbol{\xi}]\} : \boldsymbol{\chi}[\delta\boldsymbol{\xi}] - \boldsymbol{g}(\boldsymbol{\xi}) \vdots \delta\boldsymbol{\xi}] \, \text{d}\Omega - l^{(\xi)}(\delta\boldsymbol{\xi}) = 0, \tag{2.12}$$

for suitable test functions $\delta\boldsymbol{u}$ and $\delta\boldsymbol{\xi}$, where $\boldsymbol{\chi}[\boldsymbol{\xi}] \stackrel{\text{def}}{=} \boldsymbol{\xi} \cdot \boldsymbol{\nabla}$ and, $l^{(u)}(\delta\boldsymbol{u})$ and $l^{(\xi)}(\delta\boldsymbol{\xi})$ are defined in Eqs. (2.14) and (2.15). Curly brackets $\{\diamond\}$ denote implicit dependence of the argument.

Local: Find $\boldsymbol{\epsilon}^{\mathrm{p}\mathrm{l}}(\boldsymbol{x})$, such that:

$$\boldsymbol{R}_{\mathrm{L}}(\boldsymbol{u},\boldsymbol{\xi},\boldsymbol{\epsilon}^{\mathrm{p}}) \overset{\mathrm{def}}{=} \boldsymbol{\epsilon}^{\mathrm{p}} - \Delta t \frac{\partial \phi^*}{\partial \boldsymbol{\kappa}^{\mathrm{di}}}(\boldsymbol{\sigma}(\boldsymbol{\epsilon}[\boldsymbol{u}],\boldsymbol{\epsilon}^{\mathrm{p}}) + \boldsymbol{\chi}[\boldsymbol{\xi}]) - {}^{n}\boldsymbol{\epsilon}^{\mathrm{p}} = \boldsymbol{0}, \tag{2.13}$$

for known values of $\boldsymbol{u}(\boldsymbol{x})$ and $\boldsymbol{\xi}(\boldsymbol{x})$ (or else, of $\boldsymbol{\epsilon}[\boldsymbol{u}]$ and $\boldsymbol{\chi}[\boldsymbol{\xi}]$) at the integration points.

The boundary terms, $l^{(u)}(\delta\boldsymbol{u})$ and $l^{(\xi)}(\delta\boldsymbol{\xi})$, in Eqs. (2.11) and (2.12) read

$$l^{(u)}(\delta\boldsymbol{u}) = \int_{\partial\Omega_{\mathrm{t}}} \boldsymbol{t}_{\mathrm{p}} \cdot \delta\boldsymbol{u}\, \mathrm{d}\Gamma, \tag{2.14}$$

$$l^{(\xi)}(\delta\boldsymbol{\xi}) = -\int_{\partial\Omega_{\mathrm{k}}} \boldsymbol{\epsilon}_{\mathrm{p}}^{\mathrm{p}} : \boldsymbol{p}[\delta\boldsymbol{\xi}]\, \mathrm{d}\Gamma. \tag{2.15}$$

The appropriate boundary conditions that need to be prescribed become apparent from the structure of the linear forms in Eqs. (2.14) and (2.15). Discretization of the global system in Eqs. (2.11) and (2.12) leads to the finite element (global) equations. The FE-equations are solved together with local equation (2.13) via a nested iterations strategy which is described in detail in paper B [2].

2.2.2 Configurational motion problem

The thermodynamically consistent definition of the crack-driving force based on configurational forces derived in [31] is adopted here. More specifically, the total configurational force, $\boldsymbol{\mathcal{G}}$, is split into a configurational, $\boldsymbol{\mathcal{G}}^{\mathrm{CONF}}$, and a material dissipation part, $\boldsymbol{\mathcal{G}}^{\mathrm{MAT}}$. These forces in a small strain setting for a local constitutive theory read

$$\boldsymbol{\mathcal{G}}^{\mathrm{CONF}} = \int_{\Omega} -(\boldsymbol{\nabla}\overline{W}) \cdot \boldsymbol{\Sigma}\, \mathrm{d}\Omega, \tag{2.16}$$

$$\boldsymbol{\mathcal{G}}^{\mathrm{MAT}} = \int_{\Omega} -\frac{\partial \psi}{\partial \boldsymbol{\epsilon}^{\mathrm{p}}} : [\boldsymbol{\epsilon}^{\mathrm{p}} \otimes \boldsymbol{\nabla}]\overline{W}\, \mathrm{d}\Omega, \tag{2.17}$$

where $\boldsymbol{\Sigma} \overset{\mathrm{def}}{=} \psi\boldsymbol{I} - \boldsymbol{H}^{\mathrm{T}} \cdot \boldsymbol{\sigma}$ is the Eshelby energy momentum tensor, $\boldsymbol{H}(\boldsymbol{x},t) = \boldsymbol{u} \otimes \boldsymbol{\nabla}$, and $\overline{W}$ is a sufficiently smooth function that scales the configurational motion.

As regards gradient-enhanced constitutive theory adopted here, the expression for $\boldsymbol{\mathcal{G}}^{\mathrm{CONF}}$ remains the same as in Eq. (2.16), whereas $\boldsymbol{\mathcal{G}}^{\mathrm{MAT}}$ takes the form,

$$\begin{aligned}\boldsymbol{\mathcal{G}}^{\mathrm{MAT}} &= \int_{\Omega} \left[-\frac{\partial \psi}{\partial \boldsymbol{\epsilon}^{\mathrm{p}}} : [\boldsymbol{\epsilon}^{\mathrm{p}} \otimes \boldsymbol{\nabla}] - \frac{\partial \psi}{\partial \boldsymbol{g}} \vdots [\boldsymbol{g} \otimes \boldsymbol{\nabla}] \right] \overline{W}\, \mathrm{d}\Omega, \\ &= \int_{\Omega} \left[\boldsymbol{\sigma} : \boldsymbol{g} - \boldsymbol{\xi} \vdots [\boldsymbol{g} \otimes \boldsymbol{\nabla}] \right] \overline{W}\, \mathrm{d}\Omega, \end{aligned} \tag{2.18}$$

where the last equality follows from Eqs. (2.1) and (2.2), and the definition of $\boldsymbol{g}[\boldsymbol{\epsilon}^{\mathrm{p}}]$. An advantage of the proposed mixed-dual variational formulation is clearly viewed from Eq. (2.18), where all the necessary quantities for the computation of $\boldsymbol{\mathcal{G}}^{\mathrm{MAT}}$ are known already from the solution of the primary problem (Eqs. (2.11)–(2.13)). This is contrasted to the relevant expression for local theory Eq. (2.17). There, proper nodal smoothing of $\boldsymbol{\epsilon}^{\mathrm{p}}$ from known values at the integration points is required at the post-processing.

The response of the proposed gradient-enhanced mixed-dual formulation as $l_\mathrm{s} \to 0$ is of interest and it is compared here to local theory ($l_\mathrm{s} = 0$) based on a displacement-based variational formulation. For the latter formulation, perfect viscoplastic material of Bingham type is used, with the free energy, $\psi = \psi^\mathrm{loc}(\boldsymbol{\epsilon}, \boldsymbol{\epsilon}^\mathrm{p})$, where ψ^loc corresponds to the first term at the right-hand side of Eq. (2.3). Application of the gradient-enhanced mixed-dual formulation is demonstrated below for the case of a discrete singularity.

2.2.3 Application of the gradient-enhanced mixed formulation

The problem of the single edge-cracked specimen is considered here. Vertical displacement, u_2, of the upper boundary of the specimen while keeping the bottom boundary fixed is the primary problem solved for, see Fig. 2.2a. To complete the statement of boundary conditions, the effects of "hard", $\boldsymbol{\epsilon}^\mathrm{p} = \mathbf{0}$, or, "free", $\boldsymbol{p} = \mathbf{0}$, boundary conditions along the boundaries are investigated. The chosen values of all the material parameters entering the gradient-enhanced constitutive model were typical for steel and are given in paper B [2]. As mentioned in the end of the previous section, several values of l_s are investigated in this example, with the response at the limit, $l_\mathrm{s} \to 0$, being of primary importance.

(a) *Single edge-cracked specimen.*

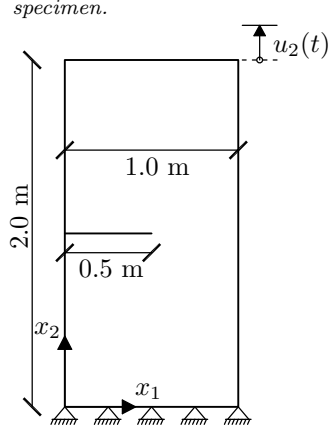

(b) *Values of* $\overline{W}$.

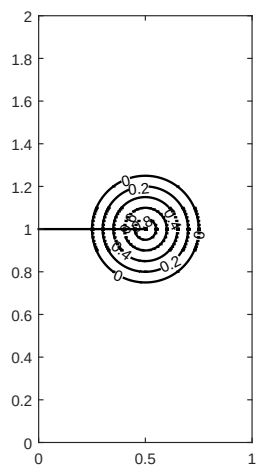

Figure 2.2: *Description of the primary problem and configurational motion.*

The considered configurational motion is virtual unit crack advance in the tangential to the crack-tip direction. The pertinent configurational motion is scaled by $\overline{W}$, whose distribution is depicted in Fig. 2.2b. As can be seen from Eqs. (2.16) and (2.18), computation of the configurational force is based on resolved fields from the solution of the primary problem stated above. In what follows, the mesh sensitivity of the energy release rates from the aforementioned configurational motion is examined. In fracture mechanics, projection of the configurational force onto the direction tangential to the crack-tip corresponds to the energy release rate due to virtual unit crack advance in this direction and is here denoted $\mathcal{G}_\parallel$. In case of linear elasticity, this projection corresponds

to the J-integral.

The computed energy release rates for varying values of l_s and for "hard" boundary conditions, $\boldsymbol{\epsilon}^\mathrm{p} = \mathbf{0}$, are shown in Fig. 2.3. The model based on the proposed gradient-enhanced formulation results in computatable rates, $\mathcal{G}_\parallel^\mathrm{CONF}$ and $\mathcal{G}_\parallel^\mathrm{MAT}$, with mesh-refinement. The behaviour for local theory is seemingly[3] not approached by the gradient-enhanced model for $l_\mathrm{s} \to 0$, as depicted in Fig. 2.4a for "hard" boundary conditions. As similar behaviour was obtained for "free" boundary conditions (see paper B [2]). The rate of congervence of the relative error in $\mathcal{G}_\parallel^\mathrm{MAT}$ with respect to ratio, l_s/h, is depicted in Fig. 2.4b for "hard" boundary conditions. Quadratic or higher rates of convergence are observed and similar rates were obtained for "free" boundary conditions (see paper B [2]).

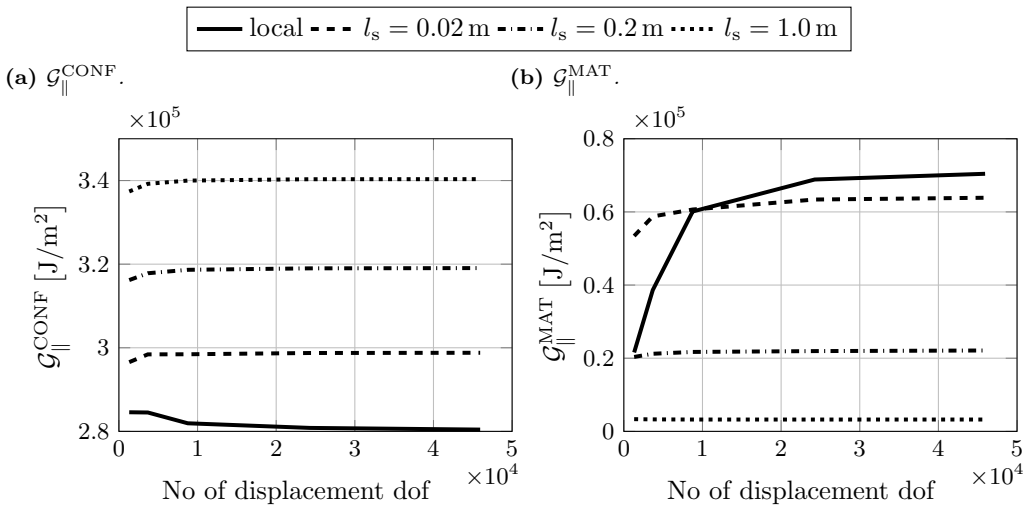

Figure 2.3: *Energy release rates at the last incremental loading step, obtained via local and gradient-enhanced constitutive theory. Case of "hard" boundary conditions,* $\boldsymbol{\epsilon}^\mathrm{p} = \mathbf{0}$.

2.3 The effect of mixed-mode loading on fatigue crack growth

2.3.1 Mixed-mode fatigue crack growth experiments

Mixed-mode fatigue crack growth due to combined axial and torsional loading occurs frequently in engineering components, see e.g. Fonte and Freitas [37]. The cyclic loads may act both in- or out-of-phase. Combinations of static torsion on top of cyclic axial load or static axial load on top of cyclic torsion are also common. RCF cracks in rails and fatigue cracks in railway axles grow under non-proportional load cycles comprised of

[3]The value of $\mathcal{G}_\parallel^\mathrm{MAT}$ for local theory does not converge to a finite value for the employed mesh resolution. Thereby, it was not possible to decide whether the behaviour of the gradient-enhanced model approaches that for local theory as $l_\mathrm{s} \to 0$.

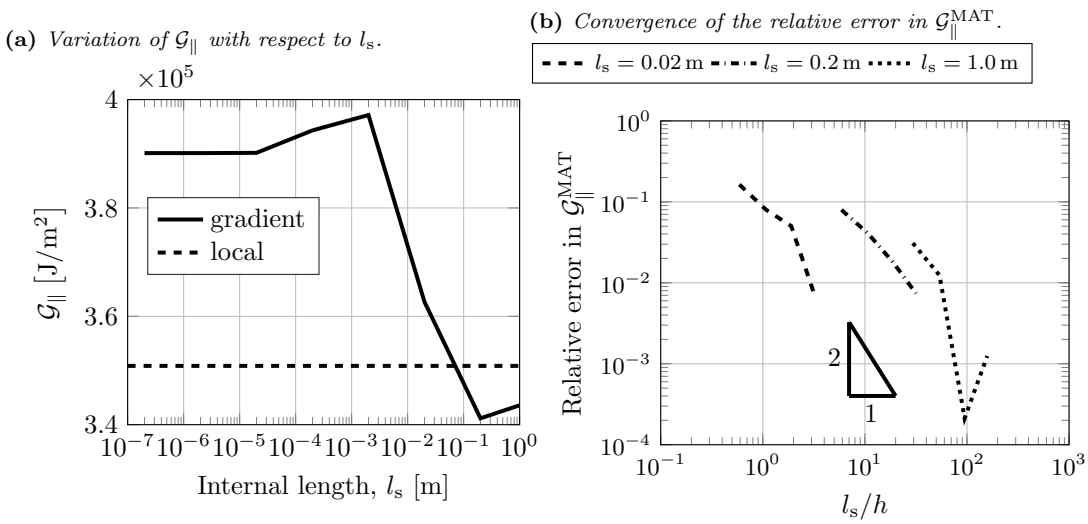

Figure 2.4: *Convergence properties of the gradient-enhanced model for the problem of the single edge-cracked specimen. Case of "hard" boundary conditions,* $\boldsymbol{\epsilon}^\mathrm{p} = \mathbf{0}$.

axial and in- and out-of-plane shear crack loading. A survey of the effect of each of the aforementioned load combinations on fatigue crack growth (rates and fracture surfaces) was conducted in paper A [1]. The principal findings are summarized below.

1. **Static torsion reduces and static tension increases the fatigue crack growth rate**.

   Experiments in the literature featuring circumferentially notched and pre-cracked solid bars subjected to a cyclic axial load on top of static torsion exhibit significantly reduced crack growth rates as compared to a pure cyclic axial load, see Fonte et al. [38], Freitas et al. [39] and Yang et al. [40]. Inclined ridges that form at the fracture surfaces and crack-closure phenomena due to a) interlocking of the ridged fracture surfaces, and b) increased plastic zone size in the vicinity of the crack-tip induced by the added static torsion, are the mechanisms presumed to govern the decrease in crack growth rates, see also Brown et al. [15].

   As regards static tension on top of cyclic torsion, superimposition of a static axial load is expected to "open" the crack and suppress the crack-closure effects that accompany mode III crack growth. In turn, reducing the crack-closure is expected to lead to higher crack growth rates. This is verified in Brown et al. [15] and Tschegg et al. [18]. However, increasing the static tension does not result in ever increasing fatigue crack growth rates. This is since extensive static axial load eventually leads to crack-tip blunting, which reduces crack growth rates and thereby acts in competition to the increasing crack growth rates due to the suppression of the mode III crack-closure phenomena. In contrast, no effect of static tension on fatigue crack growth rate was reported in Ritchie et al. [41]. According to Tschegg and Stanzl [42], the discrepancy in the effect of static tension is attributed to the fact that the

rate in Ritchie et al. [41] was measured at a short crack length, which did not allow for the effect of crack-face friction to become significant.

2. **Cyclic torsion in-phase with cyclic axial load reduces fatigue life and increases crack growth rates compared to pure cyclic axial load**.

   In fatigue crack growth experiments [43] on a solid notched bar made from R2M carbon steel, the action of cyclic torsion in-phase with cyclic tension led to a reduction in fatigue life and an increase in crack growth rates compared to pure cyclic tension.

3. **"Factory-roof" fracture surfaces may form in the presence of torsion**.

   Inclined ridges to some 45° with respect to the crack plane (commonly referred to as "factory-roof" fracture surfaces) may form in the presence of cyclic or static torsion, see Brown et al. [15]. The ridges are indications of crack growth deviation to opening-mode growth perpendicular to the principal stress direction, see Hourlier and Pineau [44] and Zhizhong et al. [45]. Although factory-roof cracks relate to tensile-mode growth, experiments featuring cyclic torsion (possibly combined with static or cyclic axial loading) may result in shear-mode (mode III) growth. In Brown et al. [15], transition to shear-mode growth is also predicted by the maximum fatigue crack growth rate criterion, provided that LEFM can be used, despite the large plastic zone sizes caused by the cyclic torsion.

2.3.2 Modeling

Numerical model description

In paper A [1], the influence of (static and/or cyclic) torsional load combined with axial load on elastic–plastic deformation of cracks is investigated. This effect is considered highly influential in RCF cracks in rails as well as in fatigue of railway axles, which operate under combined bending and torsion. For that purpose, an FE-model of a thin-walled tubular specimen with a centric hole is developed, in the commercial FE-code Abaqus [46], see Fig. 2.5. The tube is sufficiently long such that no boundary effects are imposed from the prescribed loads and the fixed boundary conditions at the right and left ends of the tube, respectively. The diameter of the centric hole is small compared to the outer diameter of the tube in order to effectively simulate an "infinite" plate under plane stress conditions, i.e. suppressing any 3D effects. Cracks of 1 [mm] length emanating from the centric hole in circumferential and 45° inclined directions are studied.

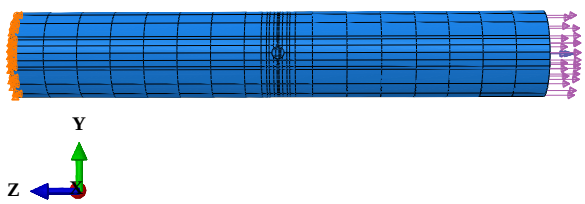

Figure 2.5: *Boundary conditions of the tubular specimen.*

A structured FE-mesh is used for discretization of the tubular specimen, which consists of second-order hexahedral elements with 3 degrees-of-freedom per node, see Fig. 2.6a. Full integration over the element volume is chosen. The mesh is graded towards the crack-tip such that the steep gradients are adequately resolved, see Fig. 2.6b.

(a) Hole and cracks region. **(b)** Crack-tip region.

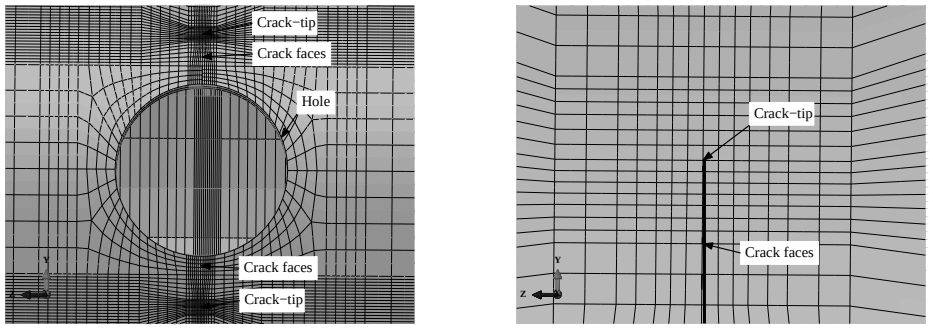

Figure 2.6: *Zoom-ins of the finite element discretization of the tubular specimen.*

The chosen length of the cracks is on the limit of macroscopically short cracks. The validity of LEFM is thus questionable [47]. It is thereby considered that elastic–plastic deformations dictate the crack growth behaviour. In this regard, elastic–perfectly plastic as well as a constitutive model featuring combined isotropic and non-linear kinematic hardening are investigated and similar conclusions regarding the effect of inelastic deformation on crack loading are drawn. The chosen material for the simulations is low-carbon steel and the material parameters that are used as input to the elastic–perfectly plastic material model follow [48] and are shown in Table 2.1.

Elastic modulus, E	185 [GPa]
Yield stress, σ_{y}	365 [MPa]
Poisson's ratio, ν	0.3

Table 2.1: Material parameters.

Measured quantities, load cases and example results

The deformation in the simulations is quantified by relative (crack-tip) displacements, δ_{I} and δ_{II}, of initially aligned node-pairs at the crack-faces, see Fig. 2.7a. The fatigue crack loading is measured by the range over the load cycle of the crack-tip displacement, $\Delta\delta$, in modes I and II, see Fig. 2.7b. The crack-tip displacements are measured at node-pair 5, some 25 [µm] away from the crack-tip.

The tube is subjected to combined stresses at the right end, as shown in Fig. 2.5. The respective load cases are described in Table 2.2.

The evolution of the ranges of elastic–plastic crack-tip displacements over the load cycles for the circumferential cracks is illustrated in Fig. 2.8. Comparing the response for

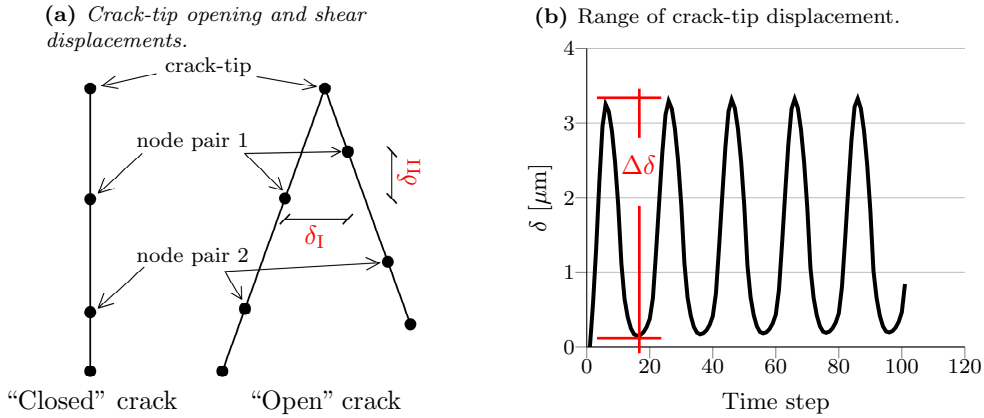

Figure 2.7: *Definitions of crack-tip displacements and range of crack-tip displacement.*

Load case	**Shear stress**	**Axial stress**
1	-	Alternating, $\sigma_a = \pm 144\,\text{MPa}$
2	Alternating, $\tau_a = \pm 144\,\text{MPa}$	–
3	Static, $\tau = 144$ MPa	Alternating, $\sigma_a = \pm 144\,\text{MPa}$
4	Alternating, $\tau_a = \pm 144\,\text{MPa}$	Static, $\sigma = 144\,\text{MPa}$
5	Alternating, $\tau_a = \pm 144\,\text{MPa}$	Alternating, $\sigma_a = \pm 144\,\text{MPa}$

Table 2.2: Employed load cases and applied stress magnitudes.

alternating axial load on top of static torsion (load case 3), with pure alternating axial load (load case 1), higher ranges of both δ_I and δ_{II} are found for the former case. However, pronounced progressive shakedown is observed for load case 3, while shakedown has occurred already at load cycle 1 in load case 1. The most detrimental (in terms of crack loading) is load case 5. The same conclusion holds also for inclined cracks configuration (see paper A [1]).

In addition, for the combined cyclic axial/static torsional load case in the literature, inclined ridges are found to form at the fracture surfaces ("factory-roof" shape), see [38] and [44]. The onset of this phenomenon is linked to a "kink" forming at the crack-tip. The pertinent deformation pattern is captured by FE-simulations, see e.g. Fig. 2.9a (paper A [1]) and [38] (cf. the crack blunting forming for the same load case in the models with inclined cracks, see Fig. 2.9b). Further discussions on all the load cases mentioned in Table 2.2 are found in paper A [1].

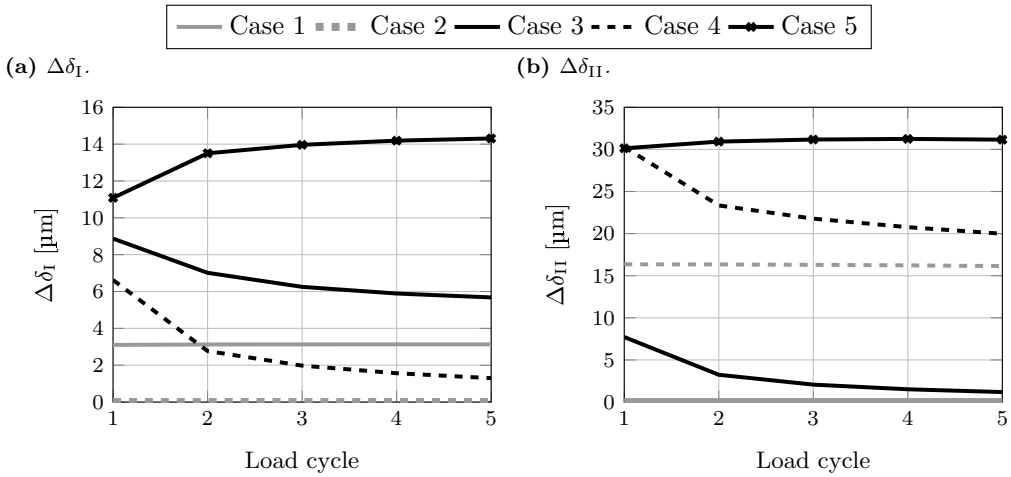

Figure 2.8: *Range of elastic–plastic crack-tip displacements for node pair 5 (for circumferential cracks).*

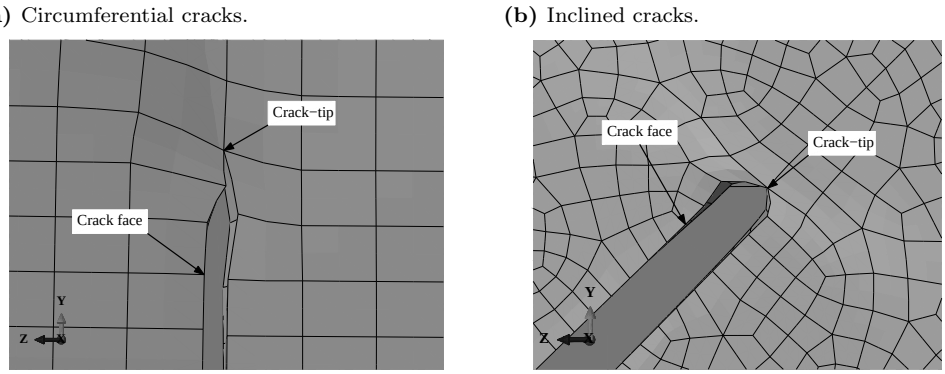

Figure 2.9: *Crack deformation under combined static torsion/alternating axial load at maximum tensile applied stress.*

2.4 Conclusions on the effect of elastoplastic deformations on crack loading

Basic pathologies regarding the most commonly employed crack-driving force parameters in the literature are identified in the review of Section 2.1. In addition, highlights from a survey on the effect of mixed-mode loading on fatigue crack growth are reiterated in Section 2.3.1. Below, a summary is provided of how the work in this thesis is positioned towards the aforementioned observations and pathologies:

1. **Static torsion reduces and static tension increases the fatigue crack**

growth rate.

In case of static torsion on top of cyclic axial load, the elastic–plastic simulations resulted in shakedown of the range of the crack-tip displacements, $\Delta\delta_{\mathrm{I}}$ and $\Delta\delta_{\mathrm{II}}$, over the load cycles. This was linked to the reduction in crack growth rates observed in the experiments for this load case, see e.g. [38] and [39]. Crack-closure and crack-face interference phenomena, intensified by torsion, were the primary causes identified in the literature for the crack growth rate reduction. The shakedown in the simulations is attributed to the kinking of the crack induced by the static torsion. Deviation of the crack growth direction is translated to a decrease in the crack-driving force available to propagate the inclined crack as compared to a straight crack subjected to a cyclic axial load perpendicular to the crack axis.

2. **Cyclic torsion in-phase with cyclic axial load reduces fatigue life and increases crack growth rates compared to pure cyclic axial load**.

   Elastic–plastic simulations for cyclic torsion in-phase with cyclic axial load resulted in a ratcheting behaviour of $\Delta\delta_{\mathrm{I}}$ and $\Delta\delta_{\mathrm{II}}$. In addition, the largest magnitudes of $\Delta\delta_{\mathrm{I}}$ and $\Delta\delta_{\mathrm{II}}$ were obtained for this load case. This is consistent with results from experiments on solid notched steel bars in [43], where combined in-phase axial and torsional load leads to higher crack growth rates than pure cyclic axial load.

3. **"Factory-roof" fracture surfaces may form in the presence of torsion**.

   Extensive crack-kinking was observed in the elastic–plastic simulations under static torsion on top of cyclic axial load. This was interpreted as the onset of the formation of inclined ridges as observed in experiments.

4. **The cyclic elastic–plastic material response imposes limitations on most of the quantities that are used to measure the crack loading**.

   Other parameters than SIFs need to be considered in cases where elastic–plastic deformations govern the fatigue response. The quantities that arose in this study as candidates for measuring the fatigue crack loading are the ranges of the relative crack-tip displacements, δ_{I} and δ_{II}. More specifically, it may be argued from Section 2.3.2 and paper A [1] that it is possible to qualitatively correlate trends in crack growth rates to the evolution of the ranges of crack-tip displacements.

   The energy release rate, as determined from configurational forces for gradient-enhanced inelasticity, was also investigated as a candidate parameter for measuring the crack loading. More specifically, in Section 2.1 and paper B [2], it was shown that it is possible to overcome numerical difficulties associated with the computation of configurational forces for inelasticity in the presence of a discrete singularity (crack). This improvement comes at the cost of a larger primary problem to solve for, compared to standard local theory. That is because of the gradient field that is included as a primary variable in the FE-equations, which increases the total number of degrees-of-freedom (dof). Moreover, the energy release rate for virtual unit crack extension tangential to the crack-tip direction was found computable with mesh-refinement and, thereby, it may be used for crack growth simulations with virtual crack extension techniques. In addition, the configurational force derived in

Eqs. (2.16) and (2.18) may be used as a crack-driving force in the formulation of a criterion for crack propagation, see Section 3.2.

3 Criteria and methods for multi-axial fatigue crack path prediction

3.1 Survey of criteria for fatigue crack path prediction

Some of the most fundamental issues that were brought about by a survey of criteria for multi-axial fatigue crack path prediction in paper C [3] are reiterated in this section. More specifically, the following challenges are addressed within the existing theories for capturing the fatigue crack paths:

1. **Limited mixed-mode ratios can be handled by SIF-based criteria**.

   A plethora of studies in the literature highlights that tensile-mode SIF-based criteria such as the Maximum Tangential Stress (MTS, [49]) and Minimum Strain-Energy-Density (MSED, [50]) criteria are able to capture the tensile-mode growth satisfactorily under conditions of moderate shear-mode loading, see [51] and [52].

2. **Accounting for elastic–plastic deformations in relation to prediction of crack growth direction is not well-established**.

   SIFs are in theory limited to linear elastic bulk material response, whereas elastic–plastic deformations impose a large effect on the low-cycle fatigue behaviour. In this regard, criteria based on stress (or strain), energy and displacement measures have been proposed in the literature. An extension of the MTS criterion to elastoplasticity is proposed in [53], where the stress evaluation is performed on the basis of an elastic–plastic finite element analysis. In this approach, the preferred direction of growth may be determined from a more accurate stress state than the one determined by SIFs for linear elasticity. However, the SIFs represent the severity of the crack situation infinitesimally close to the crack-tip under elastic conditions, in contrast to the elastic–plastic stress evaluation. The Vector Crack-Tip Displacement (VCTD) criterion was proposed in [19] and is based on crack-tip displacements in opening- and shear-modes. Good predictions of the fatigue crack growth direction from experiments are reported in [19]. However, the criterion postulates a tensile crack growth mechanism, so it is not clear how well it performs for shear-mode driven fatigue crack growth, especially under non-proportional loading as in RCF. Criteria based on the energy release rate due to crack advance for inelasticity [31] as well as the extension of the classical J-integral to account for elastoplasticity [54] are most often used for capturing the instantaneous rather than the fatigue crack growth direction. The limitations of these quantities (regarding e.g. path-independence) and their cyclic counterparts are similar to the ones of the classic J-integral discussed in Section 2.1.

3. **Lack of a generally accepted criterion under non-proportional loading**.

   The main challenges imposed by non-proportional loading on fatigue crack path prediction are how to perform load cycle evaluation and the lack of a universally applicable crack-driving force parameter [35]. With various choices of crack-driving

force parameters, efforts in the literature are dedicated to establish the combined effect on crack growth of the maximum value and range of the parameter over the load cycle. In [53], the preferred direction of growth is sought between the directions indicated by the maximizations of the tangential stress and the tangential stress range. These both seem to affect the crack growth under non-proportional loading, see [55] and [56]. The maximum crack growth rate criterion is often employed in fatigue situations under non-proportional loading, since it incorporates the effects of the maxima of both the SIFs and their ranges [55]. However, it is based on SIFs and is, in theory, susceptible to the limitations of SIF-based criteria stated above. Major problems in load cycle evaluation with the SIFs are also how to scale the influence of K_{I} as compared to that of K_{II} and how to account for non-proportionality.

4. **Lack of a universally applicable criterion for RCF crack growth**.

   Although fatigue cracks most often grow in tensile-mode, shear-mode growth is another possible mechanism [57]. It is postulated in [58] that in the absence of an apparent or dominating tensile-mode mechanism, the initial growth of surface initiated cracks in rails must take place in shear-mode and that the direction of growth follows the Maximum Shear Stress (MSS, [49]) direction. This claim is also supported by numerical simulations of twin-disc experiments in [59] and [60]. However, once RCF cracks branch from shear- to tensile-mode, it is principally impossible to predict the pertinent direction of growth by the MSS criterion, as shown in Paper C [3]. Furthermore, experimental investigation of RCF crack growth is traditionally complicated by the difficulty to reproduce shear-mode growth in laboratory conditions [61]. Partly in view of this difficulty, the asperity point load mechanism was proposed in [62]. It pertains to a tensile-mode mechanism of RCF crack growth, in which cracks may initiate and propagate by the synergistic effect of rolling contact loading and a surface asperity. In the same work, the crack path is well-captured by tensile-mode criteria such as the MTS criterion. In overall, it should be emphasized that fatigue crack growth under primary compression and crack-face friction is a challenge yet to be tackled by a criterion for prediction of the RCF crack growth.

3.2 Modeling

3.2.1 Instantaneous crack growth direction criteria

Criteria based on SIFs For linear elasticity, the in-plane stress components in the vicinity of the crack-tip with respect to the polar coordinate system of Fig. 3.1 are

expanded into a series with the first terms being,

$$\sigma_{\vartheta\vartheta}(r,\vartheta) = \frac{1}{\sqrt{2\pi r}} \overbrace{\cos\frac{\vartheta}{2}\left[K_{\mathrm{I}}\cos^2\frac{\vartheta}{2} - \frac{3}{2}K_{\mathrm{II}}\sin\vartheta\right]}^{K_\sigma(\vartheta)}, \tag{3.1}$$

$$\tau_{r\vartheta}(r,\vartheta) = \frac{1}{\sqrt{2\pi r}} \underbrace{\frac{1}{2}\cos\frac{\vartheta}{2}\left[K_{\mathrm{I}}\sin\vartheta + K_{\mathrm{II}}\left(3\cos\vartheta - 1\right)\right]}_{K_\tau(\vartheta)}, \tag{3.2}$$

where K_{I} and K_{II} are the SIFs in modes I and II, respectively. The MTS criterion is

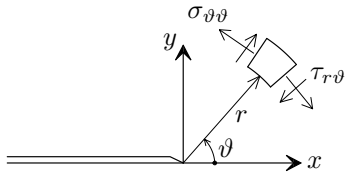

Figure 3.1: *Stress components in the plane with respect to polar coordinate system* (r,ϑ) *(*$\vartheta \in [-\pi,\pi)$ *with respect to the* x*-axis).*

based on Eq. (3.1) and postulates that the instantaneous crack growth takes place in the radial direction, perpendicular to the maximum tangential stress. According to the MSS criterion, cracks grow in the direction of maximum shear stress, determined by Eq. (3.2).

In line with the MSED criterion, the direction which minimizes the so-called strain-energy density factor is the instantaneous crack growth direction. The strain-energy-density factor is expressed as

$$S(\vartheta) = a_{11}K_{\mathrm{I}}^2 + 2a_{12}K_{\mathrm{I}}K_{\mathrm{II}} + a_{22}K_{\mathrm{II}}^2. \tag{3.3}$$

The coefficients in Eq. (3.3) are determined from

$$a_{11} = \frac{1}{16\pi\mu}\left[(1+\cos\vartheta)(\kappa-\cos\vartheta)\right], \tag{3.4}$$

$$a_{12} = \frac{1}{16\pi\mu}\sin\vartheta\left[2\cos\vartheta - (\kappa-1)\right], \tag{3.5}$$

$$a_{22} = \frac{1}{16\pi\mu}\left[(\kappa+1)\left(1-\cos\vartheta\right) + (1+\cos\vartheta)\left(3\cos\vartheta - 1\right)\right], \tag{3.6}$$

where κ is $(3-4\nu)$ for plane strain and $(3-\nu)/(1+\nu)$ for plane stress, μ is the shear modulus and ν is Poisson's ratio.

Configurational force criterion. The Configurational Force (CF) is here related to energetic changes associated with configurational changes in a continuum due to crack advance. Adopting the continuum mechanics setting in [63], the numerical counterpart of the configurational force at the crack-tip node is expressed as

$$\boldsymbol{\mathcal{G}}_a = -\int_\Omega \boldsymbol{\Sigma}\cdot\boldsymbol{\nabla}N_a\,\mathrm{d}\Omega + \int_\Omega \frac{\partial\psi}{\partial\underline{k}} \star [\sum_b \underline{k}_b \otimes \boldsymbol{\nabla}N_b]N_a\,\mathrm{d}\Omega, \tag{3.7}$$

where $\boldsymbol{\Sigma} \stackrel{\text{def}}{=} \psi \boldsymbol{I} - \boldsymbol{h}^{\mathrm{T}} \cdot \boldsymbol{\sigma}$ is the Eshelby energy-momentum tensor, N_a is the shape function associated with the crack-tip node, $\underline{k}_b$ are the nodal values of the internal variables, $\underline{k}$, at the patch of finite elements that contain the crack-tip node and N_b are the shape functions associated with the nodes of that patch. The quantities defining $\boldsymbol{\Sigma}$ are the volume-specific free energy, ψ, displacement gradient, $\boldsymbol{h} = [\boldsymbol{u} \otimes \boldsymbol{\nabla}]$ and Cauchy stress, $\boldsymbol{\sigma}$. Although, other possibilities exist, the instantaneous crack growth direction from configurational forces is determined here as the direction of $\boldsymbol{\mathcal{G}}_a$.

VCTD criterion. This criterion [19] postulates that crack growth takes place in the direction of the crack-tip displacement vector. The pertinent direction is determined as

$$\vartheta = \arcsin \frac{\delta_{\mathrm{II}}}{\delta}, \tag{3.8}$$

where δ_{I} and δ_{II} are defined in Section 2.3.2 and $\delta \stackrel{\text{def}}{=} \sqrt{\delta_{\mathrm{I}}^2 + 2\delta_{\mathrm{I}}|\delta_{\mathrm{II}}| + 2\delta_{\mathrm{II}}^2}$. A main advantage of the VCTD criterion is that it can be used irrespective of the chosen material response, since it is solely based on displacements (relate to the limitation of the SIF-based criteria to linear elastic bulk material response and the fact that CF criteria are defined only for thermodynamically consistent constitutive models).

The criteria outlined in this section may readily be used for determination of the instantaneous crack growth direction. In order to determine the fatigue crack growth direction and rate, load cycle evaluations with the criteria need to be performed. The models that are used in this thesis for load cycle evaluation are described in Sections 3.2.2 and 3.2.3.

3.2.2 Prediction of fatigue crack growth with criteria based on stress intensity factors

The fatigue crack growth direction from the SIF-based criteria is determined here via a standard approach for load cycle evaluation in the literature. The approach is described for the MTSR criterion ("R" denotes the range) in Box 3.1. The preferred fatigue crack growth direction predicted by the MTSR criterion is the direction which maximizes the range of the generalized SIF [64], K_σ, over the evaluated load cycle. Load cycle evaluation for remaining SIF-based criteria is performed in a similar way with the difference that other SIF measures are optimized, depending on the criterion.

1. A sufficiently large set of potential crack growth directions, $\vartheta \in [-\pi, \pi)$, is considered.
2. For each considered direction, we compute the range,

$$\Delta K_\sigma(\vartheta) = K_{\sigma,\max_t}(\vartheta) - K_{\sigma,\min_t}(\vartheta), \tag{3.9}$$

where

$$K_{\sigma,\max_t}(\vartheta) = \max_t \{K_\sigma(K_{\mathrm{I}}(t), K_{\mathrm{II}}(t), \vartheta)\}, \tag{3.10}$$

$$K_{\sigma,\min_t}(\vartheta) = \min_t \{K_\sigma(K_{\mathrm{I}}(t), K_{\mathrm{II}}(t), \vartheta)\}. \tag{3.11}$$

3. The preferred direction of growth is determined by

$$\varphi = \operatorname*{argmax}_{\vartheta'} \{\Delta K_\sigma(\vartheta')\}. \tag{3.12}$$

Box 3.1: Framework for prediction of crack growth direction using the MTSR criterion.

Fatigue crack growth rate

Prediction of fatigue crack growth rate using a SIF-based criterion may also be performed based on the model for load cycle evaluation outlined in Box 3.1. In case of the MTSR criterion, the range, $\Delta K_\sigma(\varphi)$, may be used as the crack-driving force parameter in a Paris-type model for crack propagation,

$$\frac{\mathrm{d}a}{\mathrm{d}N} = C\left(\Delta K_\sigma(\varphi)\right)^m \tag{3.13}$$

where a is the crack length, N is the number of load cycles and, C and m are material parameters. Equation (3.13) may then be used to assess correlation towards experimentally found fatigue crack growth rates, which provide a quantification of the suitability of the crack-driving force parameter from each criterion.

3.2.3 Prediction of fatigue crack growth with criteria based on energy and displacement measures

That fatigue crack growth takes place in small increments during loading is both intuitive as well as supported by experiments, see e.g. [65] and [66]. This can be contrasted to the standard approach for load cycle evaluation in the literature which is based on ranges over the load cycle of the quantities that are used for measuring the crack loading. In the general crack growth case, the computed range does not necesserily become fully effective at any instance during the evaluated load cycle. In this regard, a generic model for load cycle evaluation suitable for virtually any criterion is proposed in paper C [3]. Depending on the considered material, two types of load responses are considered:

1. **"Viscous" response**. Here, it is presumed that all steps of the load cycle may contribute to crack propagation. The contribution is related to the magnitude of the crack-driving force parameter at each step. The crack-driving force corresponding to a load cycle, $\Delta\boldsymbol{a}$, can then be expressed as

$$\Delta\boldsymbol{a} = \int A(t)\hat{\boldsymbol{e}}(t)\,\mathrm{d}t, \tag{3.14}$$

where t spans over the evaluated load cycle and $A(t)$ and $\hat{\boldsymbol{e}}(t)$ are the instantaneous crack-driving force parameter and crack growth direction, respectively. The definitions of $A(t)$ and $\hat{\boldsymbol{e}}(t)$ depend on the employed criterion.

2. **"Rate-independent" response**. Only the steps of the load cycle which result in loading of the crack are presumed to contribute to crack propagation. The contribution is presumed to relate to the magnitude of the crack-driving potential at each step. The crack-driving force during a load cycle, $\Delta\boldsymbol{a}$, can then be expressed as

$$\Delta\boldsymbol{a} = \int \langle \mathrm{d_t} A(t) \rangle \hat{\boldsymbol{e}}(t)\, \mathrm{d}t, \tag{3.15}$$

where $\langle \bullet \rangle \stackrel{\text{def}}{=} 1/2(\bullet + |\bullet|)$ and $\mathrm{d_t}\bullet$ denotes the time derivative.

The conceptual difference between the two types of evaluations is illustrated in Fig. 3.2. Accounting for Eqs. (3.14) and (3.15), we may express the unit vector $\hat{\boldsymbol{e}}_\varphi$ pertinent to the direction of propagation, φ, as

$$\hat{\boldsymbol{e}}_\varphi = \frac{\Delta\boldsymbol{a}}{|\Delta\boldsymbol{a}|}. \tag{3.16}$$

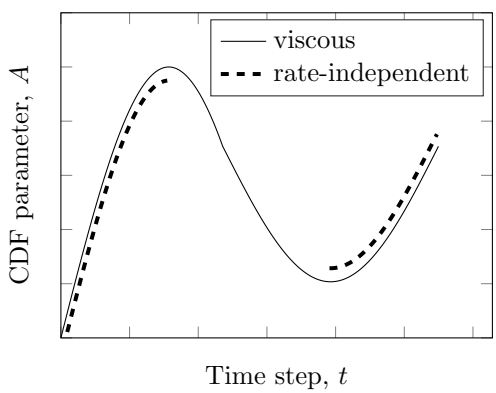

Figure 3.2: *Steps of the load cycle that are presumed to contribute to crack propagation depending on the considered type of load response.*

Remark 1. *In the literature, the crack growth increment is commonly denoted by* $\Delta\boldsymbol{a}$*. However, in this thesis,* $\Delta\boldsymbol{a}$ *denotes the resulting crack-driving force from load cycle evaluation with the criteria (Eqs.* (3.14) *and* (3.15)*).*

Crack growth rate

It is possible to extend the model for load cycle evaluation introduced in this section to also predict the fatigue crack growth rate. In this regard, the following scalar parameter

is considered,

$$|\Delta \boldsymbol{a}| = \begin{cases} |\int A(t)\hat{\boldsymbol{e}}(t)\,\mathrm{d}t|, & (\text{“viscous”}) \\ |\int \langle \mathrm{d_t} A(t)\rangle \hat{\boldsymbol{e}}(t)\,\mathrm{d}t|, & (\text{“rate-independent”}). \end{cases} \tag{3.17}$$

This parameter may then be used for evaluation of the fatigue crack growth rate via a Paris-type model for crack propagation,

$$\frac{\mathrm{d}a}{\mathrm{d}N} = C\left(|\Delta \boldsymbol{a}|\right)^m, \tag{3.18}$$

where C and m are material parameters for calibration.

3.3 Evaluation of mixed-mode fatigue crack growth direction criteria

3.3.1 Framework for evaluation of criteria

In paper C [3], a framework for evaluation of mixed-mode crack growth direction criteria and comparisons towards fatigue crack growth experiments is developed. The framework is illustrated schematically in Fig. 3.3. In short, mixed-mode fatigue crack growth experiments from the literature with well-defined crack paths are identified, as in the case of the experiment on a Compact Tension–Shear (CTS) specimen in [67], see Fig. 3.3a. The full crack path documented in each experiment (see Fig. 3.3b) is digitized via image processing [68]. An FE-model of the experiment is developed and the full crack path is embedded in the FE-mesh, see Fig. 3.3c. Simulations of the experiment are performed at chosen instances of the crack propagation. The corresponding crack length at a chosen instance is realized via enforcement of crack-face constraints at the dormant part of the crack. Based on resolved fields from the simulations, load cycle evaluations with the five crack growth direction criteria outlined in Section 3.2.1 are performed and predictions from the criteria are compared to the experimentally found crack path, see Fig. 3.3d.

The framework outlined in this section is henceforth implemented on two experiments featuring tensile-mode growth (Sections 3.3.2 and 3.3.3) and stable shear-mode growth under rolling contact conditions (Section 3.3.4). Evaluation of the criteria on these experiments and three more experiments featuring tensile-mode growth, stable shear-mode growth and shear-mode growth followed by crack-kinking to tensile-mode growth is performed in paper C [3]. Towards the last examined experiment, the effect of most complicating factors present in an RCF crack growth setting are included.

Of the evaluated criteria, the MTS, MSS and MSED criteria are based on SIFs. Load cycle evaluations with these SIF-based criteria are performed using the approach described in Section 3.2.2. In the following, the SIF-based criteria are abbreviated as MTSR, MSSR and MSEDR, where “R” denotes the range. Furthermore, the CF and VCTD criteria are also evaluated, using the generic model outlined in Section 3.2.3. All criteria and load cycle evaluation models are described in detail in paper C [3]

(a) *Mixed-mode fatigue crack growth experiment.*

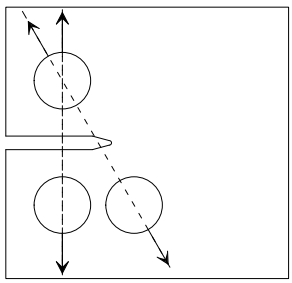

(b) *Spatial characterization of the full crack path.*

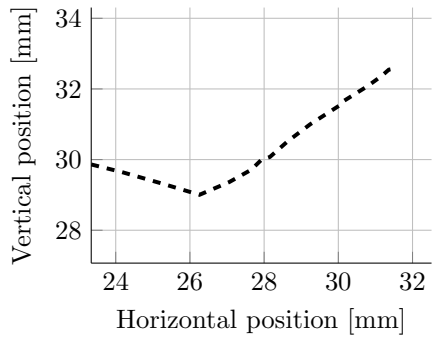

(c) *Numerical modeling of experiment.*

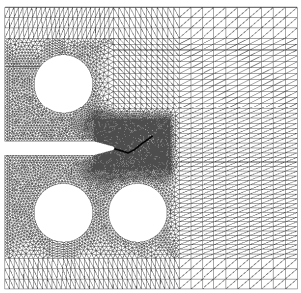

(d) *Prediction of fatigue crack growth directions and comparison to experiment.*

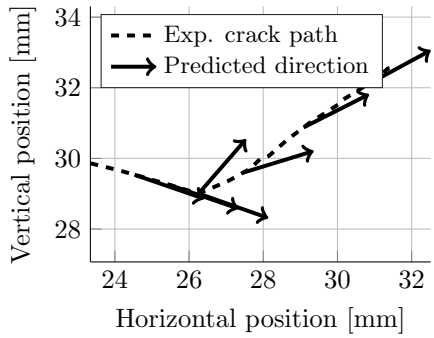

Figure 3.3: *Schematic representation of the framework for evaluation of fatigue crack growth direction criteria.*

3.3.2 Application of the framework for tensile-mode growth

Evaluation of the criteria for simulations of the tensile-mode fatigue crack growth experiment in [67] is reviewed here. The experiment is performed on a CTS specimen made of Q345R (former 16MnR) steel, see Fig. 3.4a. During crack propagation, the local propagation direction is denoted by φ and measured as the (counter-clockwise) direction from the x-axis. Pulsating load in two configurations is imposed. In the first configuration, the specimen is pulled along the y-axis by P_1, leading to the slightly inclined part of the full crack path, in some $\varphi \approx -16°$, see Fig. 3.4c. In the second configuration, the loading is inclined in $\beta = 30°$ from the y-axis (loads $P_2 - P_2$), such that the part of the crack path with $\varphi \approx 35°$ is formed.

Linear elastic simulations of the experiment described above are performed at seven instances of the propagation of the crack depicted in Fig. 3.4c. Plane stress conditions are assumed, due to the small thickness of the specimen and the in-plane loading. Young's modulus and Poisson's ratio are set to, $E = 210\,[\text{GPa}]$ and $\nu = 0.31$, respectively, in

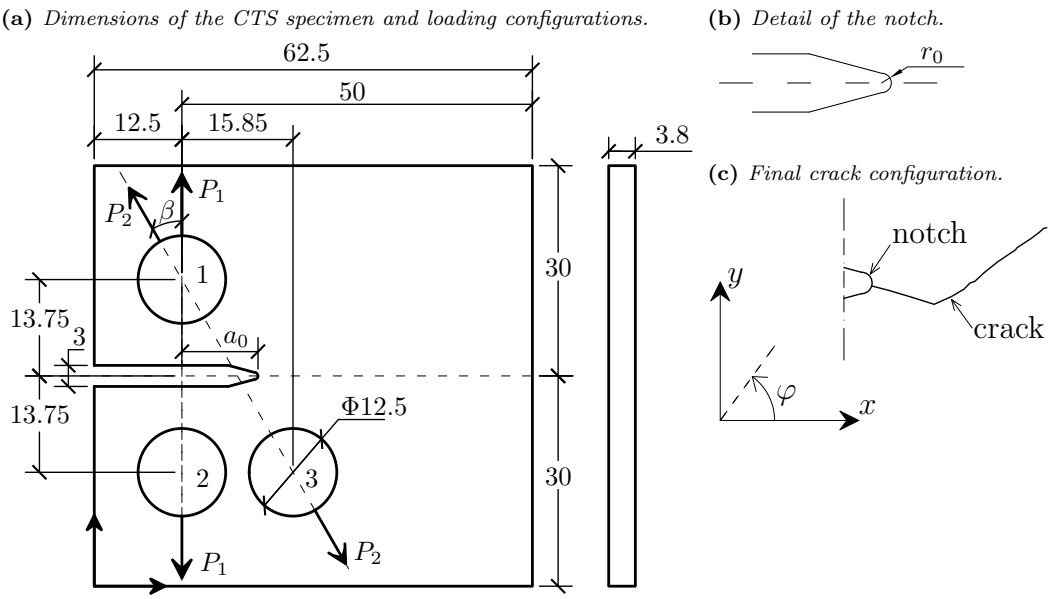

Figure 3.4: *Setting of the CTS experiment in [67].*

accordance to the calibrated material parameters for Q345R steel provided in [67].

Based on resolved fields from the simulations, the fatigue crack growth criteria are evaluated and compared to the experimentally found crack growth directions in Fig. 3.5. Results for "rate-independent" evaluation are shown in the figure. The VCTD and CF criteria accurately capture the experimentally found directions throughout the entire crack propagation. An exception comprises the instance when the crack kinks due to the change in load configuration. At that instance, predictions from the MTSR and MSEDR criteria are better than the VCTD and CF criteria. The crack growth direction is captured satisfactorily by all the criteria except for the MSSR at the first part of the crack propagation (load configuration 1). The performance of the MTSR and MSEDR criteria deteriorates at the second part of the crack propagation (load configuration 2), due to the increase of the shear crack loading at this stage.

Prediction of fatigue crack growth rates

We consider again the experiment for tensile-mode crack growth depicted in Fig. 3.4. The frameworks for evaluation of the fatigue crack growth rate with the MTSR, CF, and VCTD criteria outlined in Sections 3.2.2 and 3.2.3 are implemented on the rates measured in [67]. To this end, load cycle evaluations with the criteria have already been performed above for determination of the fatigue crack growth directions. Thereby, the corresponding crack-driving force parameters pertinent to Eqs. (3.13) and (3.18) have already been determined (see Eqs. (3.12) and, (3.14) and (3.15), respectively) and can readily be used in the Paris-type models for correlation against the experimental rates. Three correlation schemes are examined below:

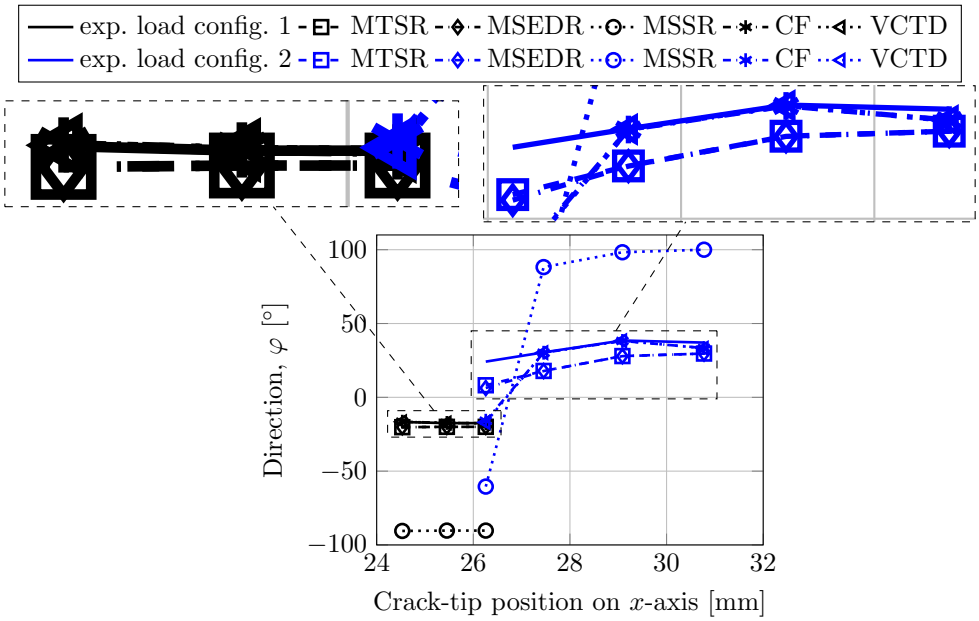

Figure 3.5: *Experimental and predicted crack growth directions for linear elastic material response of the CTS specimen experiment.*

1. Two equations (i.e. two sets of parameters, C and m) for each model defined by Eqs. (3.13) and (3.18) are fitted against the experiment; one equation for each load configuration applied in the experiment. The correlated and experimental rates are shown in Fig. 3.6a against the "true crack length", a. The latter is measured along the crack path. The crack-driving force parameters from all the three criteria correlate exactly with the experiment at load configuration 1. At load configuration 2, correlation from the VCTD criterion is more accurate than the MTSR criterion at larger crack lengths. Excellent correlation against the rates from the experiment is obtained from the CF criterion. The VCTD and MTSR criteria over-predict the crack growth rate at the instance where the crack kinks due to the change in load configuration.

2. One equation for each model is fitted against the data from both load configurations of the experiment. The correlated and experimental rates are shown in Fig. 3.6b. In this case, the correlation at load configuration 1 is not as accurate as in the first correlation scheme, especially for the CF and VCTD criteria. The quality of the correlations at load configuration 2 is similar to the quality observed in the first scheme.

3. The Paris-type models are fitted against the experiment at load configuration 1. Based on the calibrated material parameters, the crack growth rates from each criterion are then predicted at load configuration 2. Results from the pertinent

scheme are depicted in Fig. 3.6c. The predicted rates become more accurate for increasing crack length. The reason is that as the crack grows away from the kink, a more stable tensile-mode growth is established. The loading then becomes similar to the near pure opening-mode growth in load configuration 1.

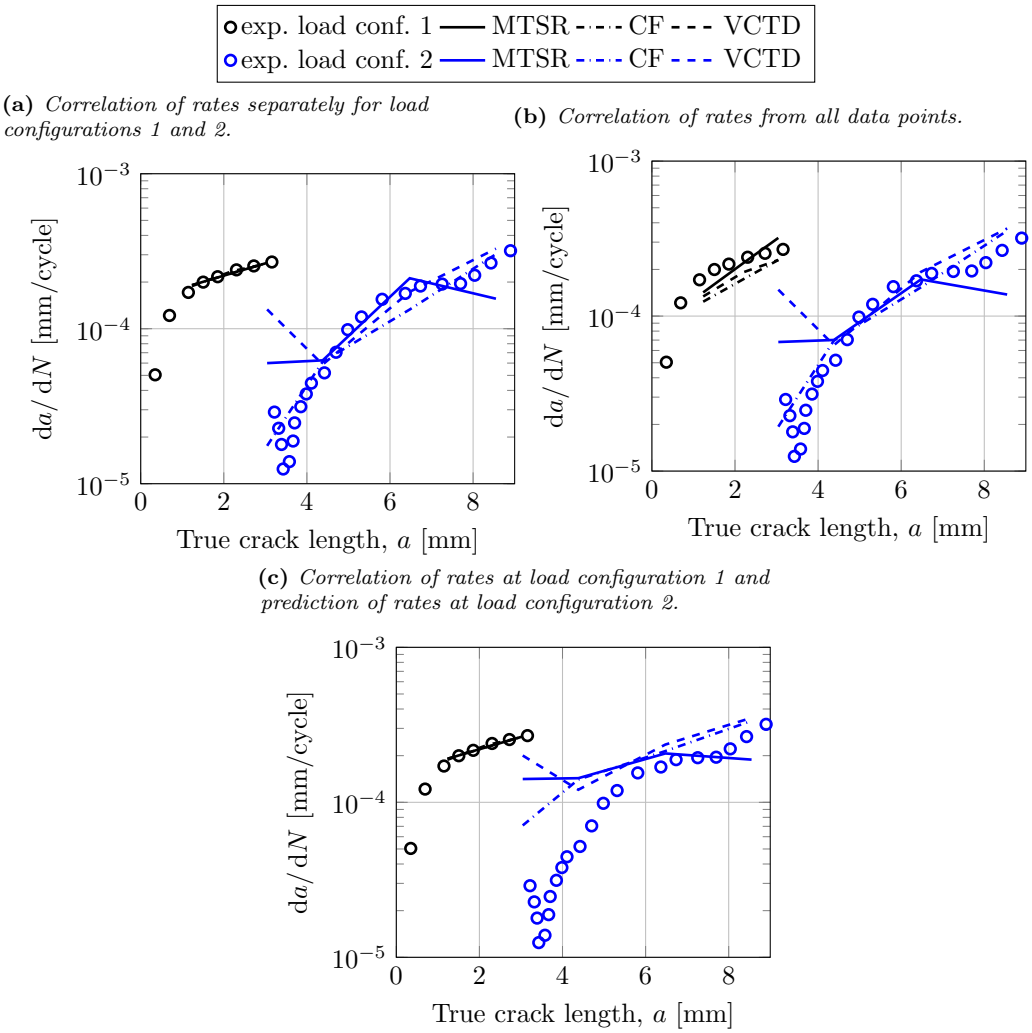

(a) *Correlation of rates separately for load configurations 1 and 2.*

(b) *Correlation of rates from all data points.*

(c) *Correlation of rates at load configuration 1 and prediction of rates at load configuration 2.*

Figure 3.6: *Correlation of crack growth rates predicted by the MTSR, CF and VCTD criteria towards experimentally found crack growth rates.*

3.3.3 The effect of elastic–plastic material response on fatigue crack path predictions

The effect of elastic–plastic material response on the predictions from the VCTD criterion is reviewed here. Simulations of the tensile-mode fatigue crack growth experiment described in Section 3.3.2 were performed using a Jiang–Sehitoglu [69] kinematic hardening model featuring five backstresses. The model is defined in paper C [3] and the calibrated material parameters for Q345R were taken from [67]. At each studied instance of crack propagation, the simulations set off assuming a "virgin" material state, i.e. from a state where no prior loading was imposed on the specimen. That this assumption did not affect the corresponding predictions from the VCTD criterion is supported by the fact that, at each studied instance, shakedown was obtained in the evolution of δ_{I} and δ_{II} already within the first few load cycles. The shakedown resulted in rapid convergence over the load cycles of the predicted crack growth direction at each instance of the crack propagation to a constant value, close to the experimentally found direction.

The VCTD criterion was evaluated based on resolved fields from the elastic–plastic simulations. Predictions from the VCTD criterion for an elastic–plastic material response are compared towards the experimentally found directions and the corresponding predictions for a linear elastic material response in Fig. 3.7. The VCTD criterion accurately captures the crack growth direction throughout the whole fatigue life also in the case of elastic–plastic material response. As in the case of linear elasticity, the criterion cannot capture the crack-kinking angle related to the change in loading configuration. It may thus be concluded that for the examined (proportional load) case, linear elastic simulations seem to suffice for accurate prediction of the fatigue crack growth direction and that elastic–plastic simulations, although they result in good predictions, do not improve the accuracy of the predictions.

3.3.4 The effect of rolling contact conditions on fatigue crack path predictions

The effect of rolling contact conditions on the ability of the criteria to predict crack growth directions was examined in paper D [4], where the framework for evaluation of criteria (Sections 3.2.2, 3.2.3 and 3.3.1) was implemented on a twin-disc fatigue crack growth experiment [70]. The effective setting of the experiment is depicted in Fig. 3.8a. The applied pressure between the discs resulted in a maximum Hertzian contact pressure of some 1500 [MPa]. At first, 500 unlubricated cycles corresponding to a friction coefficient of some $\mu \approx 0.42$ were imposed. The full crack path documented in Fig. 3.8b emerged after the application of 31 054 lubricated cycles with $\mu \approx 0.04$. The resulting crack is inclined to some $\varphi \approx -20°$, with φ defined in Fig. 3.9.

Linear elastic plane strain simulations of the experiment described above were performed at four instances of the fatigue life of the crack depicted in Fig. 3.8b. The physical model of the experiment is shown in Fig. 3.9. A small coupon $b \times h$ of the rail disc was modeled. The coupon was large enough to prevent unwanted boundary effects. The wheel load on the rail disc was modeled as a moving Hertzian pressure distribution, $p_n(x)$, combined with a frictional load, $p_t(x) = \mu p_n(x)$, assuming full-slip conditions at the wheel–rail

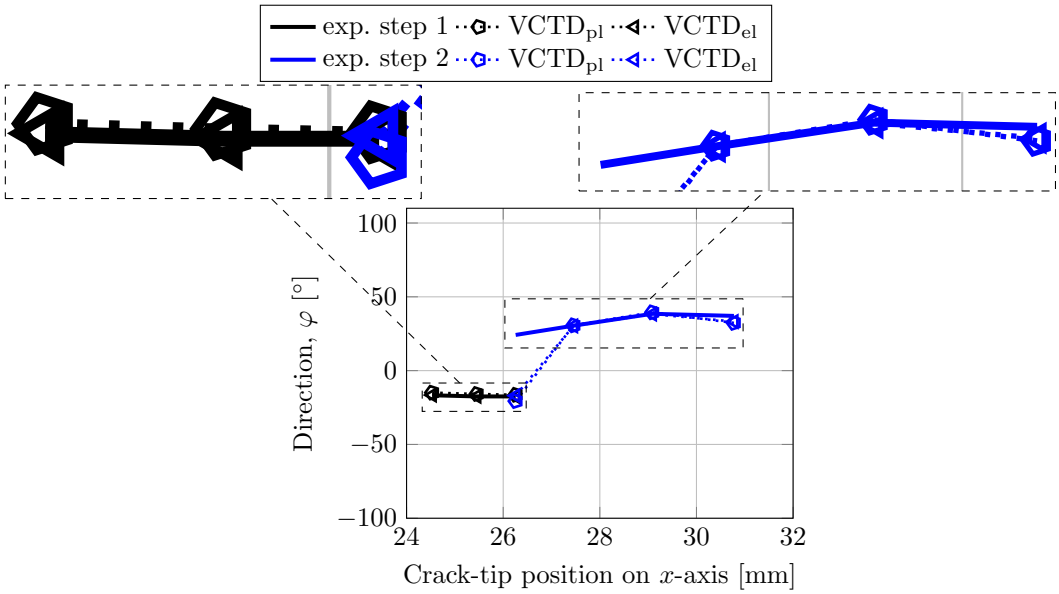

Figure 3.7: *Comparison of predictions for elastic and elastic–plastic material response.*

(a) *Specimen dimensions and loading.*

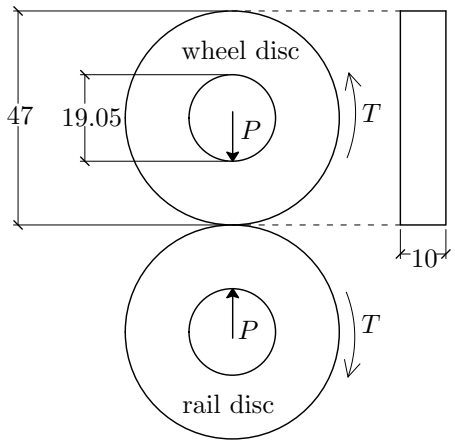

(b) *Final crack configuration.*

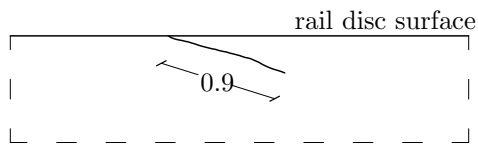

Figure 3.8: *Effective setting of the twin-disc experiment in [70] (dimensions in* [mm]*).*

contact patch. Owing to the presumption of elasticity, the model was subjected to one wheel load passage (corresponding to one rolling/sliding load cycle), which corresponds to some 30 placements of the contact load. The majority of the placements were allocated over the crack region, which is where the influence on the crack-tip fields is the largest.

The crack growth direction criteria were evaluated based on results from the simulations. Predictions from the criteria are compared to the experimentally found crack path in

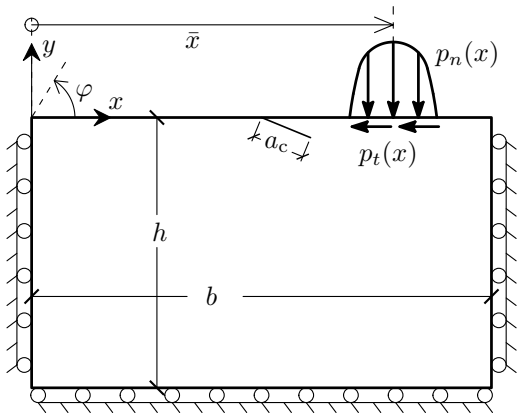

Figure 3.9: *Physical model of the twin-disc fatigue crack growth experiment.*

Fig. 3.10. The shear-mode crack growth direction observed in the experiment is very satisfactorily captured by the MSSR and VCTD criteria. Good predictions are obtained from the CF criterion only at the first two evaluated instances. Crack-kinking to tensile-mode growth is incorrectly predicted by the MTSR and MSEDR criteria at all the evaluated instances[1]. The conclusions are in principle similar to those obtained from evaluation of the criteria on the stable shear-mode crack growth experiment studied in paper C [3]. That experiment featured a cruciform specimen with a centric notch and a pre-crack emanating from the notch, subjected to remote bi-axial stresses of much smaller magnitude than the compressive stresses present at the twin-disc test. That is, the primary compression that the crack is undergoing in the twin-disc experiment seems to impose only a small effect on predictions from the criteria.

3.4 Prediction of fatigue crack paths in rails

Based on the evaluation of the criteria proposed in papers C [3] and D [4], the Vector Crack-Tip Displacement (VCTD) criterion is used to quantify crack path directions in rails under realistic railway traffic, see paper E [5]. A 2D plane strain model of the rail together with an assumed Hertzian loading including fully developed slip were used for conducting a parametric study of the preferred crack growth directions under varying operational conditions. A crack inclined in 25 [°] from the rail surface was embedded in the model. The influence of wheel load, P, amount of traction (represented by a friction coefficient, μ_{WR}, under the assumption of full-slip) and coefficient of friction at the crack-faces, μ_{CF}, were considered. The set of operational parameters that resulted in predicted directions with the best agreement towards the direction of the embedded crack was chosen as a reference case.

Predictions for the reference case and cases with varying operational parameters from the reference case are shown in Fig. 3.11. Results indicate μ_{WR} as the most influential

[1]Due to the macroscopically short crack length, the applicability of LEFM is questionable. Therefore, predictions from the SIF-based criteria should be considered with special caution in this experiment.

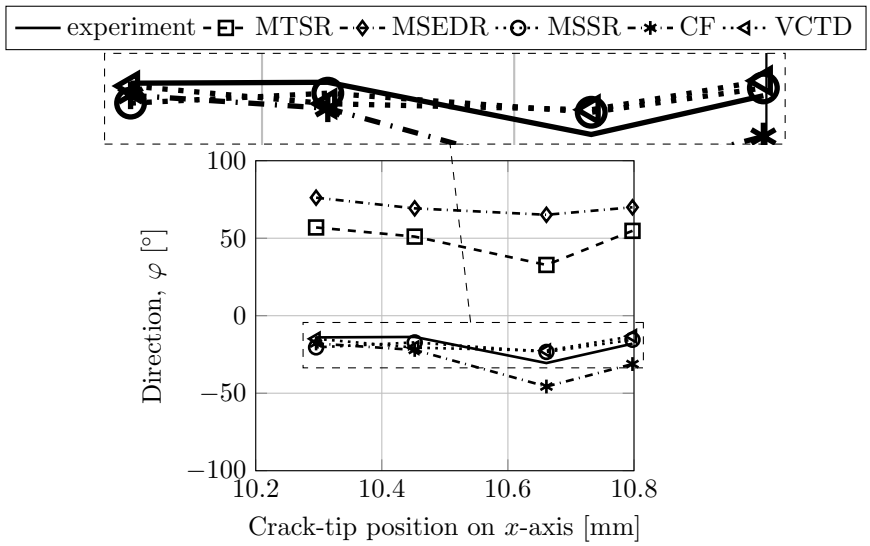

Figure 3.10: *Experimental and predicted crack growth directions for linear elastic simulations of the twin-disc fatigue crack growth experiment.*

parameter on crack growth direction predictions, see Fig. 3.11a. An upwards crack-kinking is predicted for increasing μ_{WR}. This was attributed to the combined effects of a large negative crack-tip displacement in shear-mode, δ_{II}, for increasing μ_{WR} and simultaneous crack opening that allowed for such crack-kinking to take place. In contrast, crack-face friction was found the least influential parameter, see Fig. 3.11b. This was explained by the lack of contact between the crack-faces in the vicinity of the crack-tip at the instances of maximum and minimum δ_{II} over the load cycle.

Finally, the influence of global stresses in rails, stemming from bending of the rail, was investigated. Predictions for the reference case and a case with added global bending on top of the reference wheel load are depicted in Fig. 3.12. Addition of global bending resulted in prediction of significant downwards crack-kinking. The reason for this was the significant crack opening at the end of the considered bending/rolling contact load cycle that allowed for the positive δ_{II} to become effective causing the downwards crack-kinking.

3.5 Conclusions on fatigue crack path predictions

A set of fundamental issues were highlighted in Section 3.1 regarding the commonly employed criteria in the literature for prediction of the multi-axial fatigue crack path. It is fruitful to examine the extent to which the current study succeeded in addressing the pertinent issues:

1. **Limited mixed-mode ratios can be handled by SIF-based criteria**.

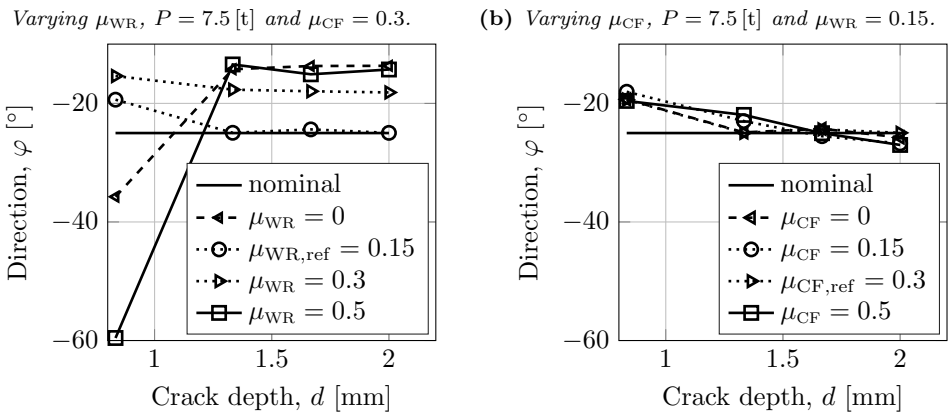

Figure 3.11: *Predicted and observed crack growth directions without consideration of global stresses. Subscript "ref" denotes the reference RCF case,* $P = 7.5$ [t], $\mu_{WR} = 0.15$ *and* $\mu_{CF} = 0.3$.

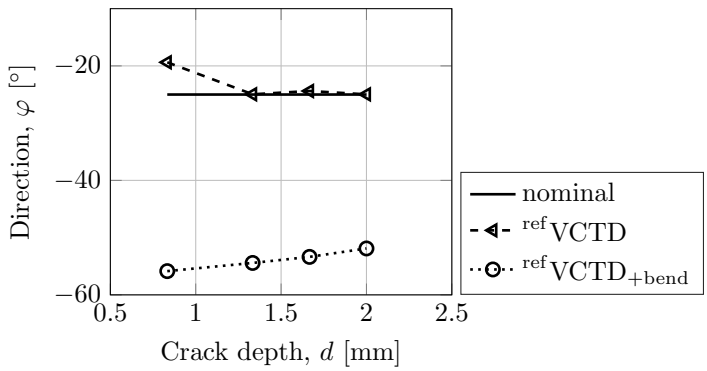

Figure 3.12: *Predicted and observed crack growth directions with and without global stresses due to bending.*

This was verified especially by the study of tensile-mode fatigue crack growth experiments in paper C [3], see also Section 3.3.2. More specifically, it was shown in Fig. 3.5 that the predictions from the MTSR and MSEDR criteria deteriorate at load configuration 2, where the shear crack loading is increased as compared to load configuration 1. On the contrary, the VCTD and CF criteria gave accurate crack path predictions throughout the whole crack growth life, i.e. irrespective of the effective mixed-mode ratio at the studied instances of the crack propagation. An issue that requires further investigation is the performance of the latter criteria at the instances when an abrupt change in load configuration takes place, a change that is enough to cause substantial kink to the crack. Possible remedies for this are proposed in Section 6.

2. **Accounting for elastic–plastic deformations in relation to prediction of crack growth direction is not well-established**.

   The effect of elastic–plastic deformation on predictions from the criteria was examined in three experiments (two of them are shown here whereas the third is described in paper C [3]). The same principles behind the proposed generic model for load cycle evaluation with the criteria were employed (see Section 3.2.3), irrespective of material response. The main conclusion is that modeling the cyclic elastic–plastic material response does not improve the accuracy of the crack path predictions. More specifically, predictions by the VCTD criterion for elastic and elastic–plastic response were similar. Moreover, linear elastic simulations were sufficient for accurate prediction of the fatigue crack path using the VCTD criterion. For the CF criterion, the effect of elastic–plastic deformation is still unclear. From this investigation, it may be argued that more research is required in the formulation of a load cycle evaluation scheme and the establishment of an appropriate crack-driving force parameter in the elastic–plastic regime.

3. **Lack of a generally accepted criterion under non-proportional loading**.

   Accurate predictions of the fatigue crack growth directions from the VCTD criterion were obtained from the evaluation of the criteria on three experiments featuring non-proportional loading in papers C [3] and D [4]. Load cycle evaluation with the VCTD criterion was based on the generic framework for load cycle evaluation outlined in Section 3.2.3. Thus, we consider the VCTD criterion combined with the proposed model for load cycle evaluation as good candidates for prediction of the fatigue crack path under non-proportional loading. Nevertheless, there are still related topics that require further investigation, as discussed in Section 6.

4. **Lack of a universally applicable criterion for RCF crack growth**.

   Simulations of two experiments that essentially resemble the RCF crack growth were performed in paper C [3]. The experiments featured stable shear-mode and shear-mode growth followed by crack-kinking to tensile-mode growth. From evaluation of the criteria in these cases, it is concluded that the VCTD criterion accurately captures the shear- and tensile-mode growth as well as the transition between these. In addition, the rolling contact conditions in the twin-disc experiment described in Section 3.3.4 and paper D [4] had a rather small effect on the performance of the criterion. Thereby, the combination of the VCTD criterion and the generic model for load cycle evaluation proposed here are considered as strong candidates for capturing the RCF crack growth. To this end, more simulations of RCF crack growth experiments need to be performed, as detailed in Section 6.

4 Finite element software development and utilization of existing software

Finite element analyses have been performed in all the appended papers of the thesis. Below is the complete list of software used for the computations:

- Preprocessing:
  - The geometries of the specimens modeled in papers B [2], C [3] and D [4] were designed in the 2D design and drafting software, Draftsight [71].
  - Image processing (e.g. of the full crack path documented in each experiment in papers C [3] and D [4]) was performed by WebPlotDigitizer [68].
  - Meshing of model geometries was performed in Abaqus [46].
  - The FE-matrices from the Abaqus mesh were imported into Matlab by an in-house developed interface code, AbaqusMesh2Matlab [72].
- Finite element analyses in paper A [1] were performed in Abaqus [46].
- Finite element analyses in papers B [2], C [3], D [4] and E [5] were performed in FE4E, an in-house functional programming code for non-linear finite element analysis written in Matlab.
- Postprocessing was performed with FE4E.

5 Summary of appended papers

5.1 Paper A: A numerical investigation of elastoplastic deformation of cracks in tubular specimens subjected to combined torsional and axial loading

A numerical investigation is performed on pre-cracked tubular specimens under combined alternating and/or static axial and torsional loading in various load configurations. The elastic–plastic deformation of the crack-faces is quantified via crack-tip displacements. The ranges of the crack-tip displacements over each load cycle effectively serve as indicators of the severity of the fatigue crack loading. Identified ratcheting effects in crack-tip displacements are linked to crack blunting, while shakedown effects indicate the build-up of residual stresses. Obtained numerical results are linked to experimental trends found in the literature. Most notably, it is shown that it is possible to correlate described trends with the evolution of the ranges of the crack-tip displacements obtained from the simulations.

5.2 Paper B: On configurational forces for gradient-enhanced inelasticity

Configurational (or material) forces are computed within a gradient-enhanced constitutive theory, based on a mixed variational formulation. The mixed formulation includes the displacements combined with a stress measure that is energy conjugated to the spatial gradient of the internal variables. An internal length measure is used as a regularization parameter.

The mesh sensitivity of the energy release rates pertinent to the computed configurational forces is examined for the case of a smooth interface and a discrete singularity. Results show that the proposed gradient-enhanced mixed formulation provides sufficient regularity for the computation of configurational forces. Furthermore, the behaviour of the gradient-enhanced model for vanishing internal length is investigated. The study concludes that the choice of boundary conditions pertinent to the gradient-enhanced formulation has a significant influence on the computed rates for vanishing internal length in the case of the smooth interface. In contrast, little effect is observed for the case of a discrete singularity. The relative error of convergence of the material dissipation part of the total energy release rate is shown to decrease quadratically (or higher) with respect to the ratio of the internal length to the characteristic element size.

5.3 Paper C: Evaluation of crack growth direction criteria on mixed-mode fatigue crack growth experiments

Crack growth direction criteria are evaluated for four mixed-mode fatigue crack growth experiments from the literature. The evaluation is based on numerical simulations of the experiments at different instances of the crack propagation. At each studied instance, load cycle evaluations featuring the different criteria are performed. To this end, a generic model for load cycle evaluation is proposed and implemented. The simulated experiments feature tensile-mode growth, stable shear-mode growth and shear-mode growth followed by crack-kinking to tensile-mode growth.

Of the evaluated criteria, the configurational force and vector crack-tip displacement criteria accurately predict the tensile-mode growth throughout the whole crack propagation. An exception to this is the predictions from these criteria at the instances where an abrupt change in load configuration is applied, which is enough to cause substantial kinking of the current crack growth direction. Predictions from criteria based on stress intensity factors are superior at these instances. However, it is shown that SIF-based criteria can only handle moderate shear crack loading (or pure shear-driven growth).

5.4 Paper D: Evaluation of mixed-mode crack growth criteria under rolling contact conditions

The performance of several mixed-mode crack growth direction criteria from the literature is investigated under rolling contact conditions. In this regard, linear elastic simulations of a twin-disc fatigue crack growth experiment from the literature are performed at different instances of the crack propagation. A two-dimensional FE-model of the rail disc is developed in plane strain. The wheel disc loading is modeled by moving Hertzian and frictional contact loads. Full-slip conditions are adopted.

Based on resolved fields from the simulations, load cycle evaluations featuring the crack growth direction criteria are performed. The previously developed generic model for load cycle evaluation is employed. Of the evaluated criteria, the vector crack-tip displacement and maximum shear stress range criteria very satisfactorily predict the shear-mode growth documented in the experiment. The configurational force criterion performs satisfactorily at shorter crack lengths. Criteria based on tensile-mode stress intensity factors such as the maximum tangential stress range and minimum strain energy density range criteria incorrectly predict crack-kinking to tensile-mode growth at all the evaluated instances of the crack propagation.

5.5 Paper E: Evaluation of rolling contact fatigue crack growth directions in rails under varying operational conditions

The effect of different operational conditions on rolling contact fatigue (RCF) crack growth direction is investigated numerically. Predicted crack growth directions are compared for pertinent wheel–rail contact conditions. The investigation is performed via a representative plane strain Finite Element (FE) model. A plate representing the rail is considered and the three-dimensional load from the wheel is appropriately transformed into a two-dimensional pressure and frictional load moving on top of the plate. A fatigue crack is embedded in the FE-mesh at an angle and until a depth which are representative of an initiated RCF crack in a rail. The studied operational scenarios feature variations in wheel load, wheel–rail friction and crack-face friction, and addition of longitudinal stresses in the rail due to bending and/or a temperature variation. Simulations are performed under the predefined scenarios at different instances of the fatigue life of the embedded crack. The resulting resolved fields are used for evaluation of the vector crack-tip displacement criterion. Results indicate wheel–rail friction coefficient as the most influential parameter on predicted crack growth directions. Crack-face friction was found the least influential parameter, due to lack of contact in the vicinity of the crack-tip at the instances of maximum and minimum shear crack-tip displacements over the load cycle.

6 Concluding remarks and future work

The effect of elastic–plastic deformation on crack loading is examined in papers A [1] and B [2]. In view of the numerical difficulties associated with the computation of configurational forces for local inelasticity, a gradient-enhanced mixed variational formulation is proposed in paper B [2] and configurational forces are computed based on this formulation. The suitability of the ranges of crack-tip displacements as quantities for measuring fatigue crack loading is investigated in paper A [1]. For this purpose, elastic–plastic simulations on pre-cracked tubular specimens are performed under various combinations of torsional and axial loading. Numerical procedures for prediction of the fatigue crack paths under multi-axial loading are developed in paper C [3]. The procedures are used for the evaluation of crack growth direction criteria based on simulations of mixed-mode fatigue crack growth experiments from the literature. The ability to predict crack growth directions under rolling contact conditions is studied in papers D [4] and E [4].

As regards prediction of the fatigue crack path, the configurational force and Vector Crack-Tip Displacement (VCTD) criteria yielded accurate predictions of the tensile-mode growth. An exception was the prediction of crack-kinking caused by a (drastic) instantaneous change in the applied load configuration, see Section 3.3.2. Due to the fact that crack-kinking may take place gradually, the way to define and measure the crack-kinking angle is not always straightforward. Nevertheless, a more focused spatial discretization at the part of the crack path where crack-kinking takes place and refined simulation of the experiments at instances of the crack propagation that kinking takes place may be a remedy towards improved prediction also of crack-kinking angles.

Furthermore, accurate predictions also of the shear-mode growth as well as the transition to and the subsequent tensile-mode growth were obtained from the VCTD criterion, see paper C [3]. Good predictions from the VCTD criterion were also obtained in simulations of a twin-disc experiment featuring shear-mode growth in paper D [4]. Despite the satisfactory predictions, RCF cracks in rails exhibit characteristics that were not present either in the studied experiments or in the numerical simulations or both. Multiple cracks with branches and non-planar crack propagation are examples. These are currently not captured by the proposed framework and need to be properly included in RCF crack path predictive models.

In addition, RCF cracks in rails propagate under primary compression. This magnifies the effect of crack-face friction. Accounting for the fact that friction-less contact between the crack-faces has been assumed throughout the initial work in this thesis, the effect of crack-face friction in all aspects of the work in this thesis should be revisited. A first attempt in this respect is presented in paper E [5]. As regards elastic–plastic deformation of cracks, crack-face friction is expected to reduce the crack-tip displacement in shear-modes. For a more pronounced effect, simulations on thick-walled members under the action of torsion combined with primary compression should preferably be considered. From a computational point of view, loaded crack-faces result in a contribution from the boundaries to the total configurational force [34]. For the gradient-enhanced mixed formulation proposed in paper B [2], it is interesting to investigate whether the presence of friction allows for computable energy release rates from projections of the internal and

boundary parts of the configurational force with mesh-refinement.

Fatigue crack growth is also affected by the cyclic elastic–plastic material response. In paper C [3], predictions from the linear elastic simulations provided results better than the ones obtained from elastic–plastic simulations. In general, linear elastic simulations seem to suffice to get accurate predictions from the VCTD criterion in papers C [3] and D [4]. In this regard, it may be argued that more research is required in the formulation of a model for load cycle evaluation in the presence of elastic–plastic deformations. In addition, there exist few constitutive models in the literature that are both thermodynamically consistent and able to capture the cyclic elastic–plastic material response of standard (rail) steel. The Chaboche [73] model adopted in paper C [3] is one example of a constitutive model that, in theory, possesses both of the aforementioned properties. However, calibration of the model parameters for standard rail steel in the literature does not fit well even against uni-axial stress experiments, see e.g. [74]. To the author's opinion, satisfactory calibration of the Chaboche model on standard rail steel is possible, provided that a proper strategy is adopted for setting the initial guess of the material parameters in the pertinent optimization problem, see paper C [3]. To this end, derivation, efficient/stable numerical solution and calibration of constitutive models that are both thermodynamically consistent as well as able to capture the cyclic elastic–plastic material response of railway steel will allow for more accurate elastic–plastic simulations and the evaluation of criteria based also on configurational forces.

Finally, in order for a framework for 2D fatigue crack growth prediction to claim completeness, both the rate and direction of growth should be predicted. Thereby, the proposed framework in paper C [3] should be extended towards prediction also of crack growth rates. Such an extension may be performed based on scalar quantities that are readily available from load cycle evaluation for prediction of the fatigue crack growth direction, as described in Section 3.2.3. A proposed procedure and a basic preliminary result was presented in this thesis. Nevertheless, even if the developed framework for evaluation of criteria pin-points towards criteria capable of capturing both fatigue crack growth direction and rate, fatigue crack growth simulations free of any bias (such as the predefined crack paths used in this thesis) require a robust computational framework. To achieve this, there is room for improvement. To-date there is for example no consensus on how the mapping of e.g. the internal variables at the integration points from the "current" to the updated mesh should be performed when loading of the crack in the current mesh exceeds the threshold value for crack propagation measured by a given criterion.

References

[1] D. Floros, A. Ekberg, and K. Runesson. A numerical investigation of elastoplastic deformation of cracks in tubular specimens subjected to combined torsional and axial loading. *International Journal of Fatigue* **91** (2016), 171–182. DOI: 10.1016/j.ijfatigue.2016.06.008.

[2] D. Floros, F. Larsson, and K. Runesson. On configurational forces for gradient-enhanced inelasticity. *Computational Mechanics* **61**.4 (2018), 409–432. DOI: 10.1007/s00466-017-1460-x.

[3] D. Floros, A. Ekberg, and F. Larsson. Evaluation of crack growth direction criteria on mixed-mode fatigue crack growth experiments. *Submitted for international publication* (2018).

[4] D. Floros, A. Ekberg, and F. Larsson. "Evaluation of mixed-mode crack growth criteria under rolling contact conditions". *Proceedings of the 11th International Conference on Contact Mechanics and Wear of Rail/Wheel Systems*. TU Delft, 2018, pp. 253–260.

[5] D. Floros, A. Ekberg, and F. Larsson. Evaluation of rolling contact fatigue crack growth directions in rails under varying operational conditions. *To be submitted for international publication* (2018).

[6] M. Marshall, R. Lewis, R. Dwyer-Joyce, U. Olofsson, and S. Björklund. Experimental characterization of wheel-rail contact patch evolution. *Journal of Tribology* **128**.3 (2006), 493–504. DOI: 10.1115/1.2197523.

[7] G. Girsch, J. Keichel, R. Gehrmann, A. Zlatnik, and N. Frank. "Advanced rail steels for Heavy Haul application-track performance and weldability". *Proceedings - 9th International Heavy Haul Conference: "Heavy Haul and Innovation Development"*. 2009, pp. 171–178.

[8] E. E. Magel. *Rolling contact fatigue: a comprehensive review*. Tech. rep. 2011.

[9] N. Larijani, J. Brouzoulis, M. Schilke, and M. Ekh. The effect of anisotropy on crack propagation in pearlitic rail steel. *Wear* **314**.1 (2014). Proceedings of the 9th International Conference on Contact Mechanics and Wear of Rail / Wheel Systems, Chengdu, 2012, 57–68. DOI: 10.1016/j.wear.2013.11.034.

[10] J. Brouzoulis. Wear impact on rolling contact fatigue crack growth in rails. *Wear* **314**.1 (2014). Proceedings of the 9th International Conference on Contact Mechanics and Wear of Rail / Wheel Systems, Chengdu, 2012, 13–19. DOI: 10.1016/j.wear.2013.12.009.

[11] A. F. Bower. The Influence of Crack Face Friction and Trapped Fluid on Surface Initiated Rolling Contact Fatigue Cracks. *Journal of Tribology* **110**.4 (1988), 704–711. DOI: 10.1115/1.3261717.

[12] J. W. Ringsberg. Shear mode growth of short surface-breaking RCF cracks. *Wear* **258**.7-8 (2005), 955–963. DOI: 10.1016/j.wear.2004.03.043.

[13] S. Wong, P. Bold, M. Brown, and R. Allen. A branch criterion for shallow angled rolling contact fatigue cracks in rails. *Wear* **191**.1 (1996). 4th International Conference on Contact Mechanics and Wear of Rail-Wheel Systems, 45–53. DOI: 10.1016/0043-1648(95)06621-7.

[14] N. E. Dowling. *Mechanical behavior of materials: engineering methods for deformation, fracture, and fatigue*. Prentice hall, 1993.

[15] M. W. Brown, E. Hay, and K. J. Miller. Fatigue at notches subjected to reversed torsion and static axial loads. *Fatigue and Fracture of Engineering Materials and Structures* **8**.3 (1985), 243–258. DOI: 10.1111/j.1460-2695.1985.tb00425.x.

[16] K. Tanaka. Fatigue crack propagation from a crack inclined to the cyclic tensile axis. *Engineering Fracture Mechanics* **6**.3 (1974), 493–507. DOI: 10.1016/0013-7944(74)90007-1.

[17] D. Rozumek and E. Macha. A survey of failure criteria and parameters in mixed-mode fatigue crack growth. *Materials Science* **45**.2 (2009), 190. DOI: 10.1007/s11003-009-9179-2.

[18] E. K. Tschegg, S. E. Stanzl, H. R. Mayer, and M. Czegley. Crack face interactions and near-threshold fatigue crack growth. *Fatigue and Fracture of Engineering Materials and Structures* **16**.1 (1993), 71–83. DOI: 10.1111/j.1460-2695.1993.tb00071.x.

[19] C. Li. Vector ctd criterion applied to mixed mode fatigue crack growth. *Fatigue and Fracture of Engineering Materials and Structures* **12**.1 (1989), 59–65. DOI: 10.1111/j.1460-2695.1989.tb00508.x.

[20] E. Tschegg. The influence of the static I load mode and R ratio on mode III fatigue crack growth behaviour in mild steel. *Materials Science and Engineering* **59**.1 (1983), 127–137. DOI: 10.1016/0025-5416(83)90094-0.

[21] J. R. Rice. A path independent integral and the approximate analysis of strain concentration by notches and cracks. *Journal of applied mechanics* **35**.2 (1968), 379–386. DOI: 10.1115/1.3601206.

[22] N. Dowling and J. Begley. "Fatigue crack growth during gross plasticity and the J-integral". *Mechanics of crack growth*. ASTM International, 1976, pp. 82–103. DOI: 10.1520/STP33940S.

[23] K. Tanaka. The cyclic J-integral as a criterion for fatigue crack growth. *International Journal of Fracture* **22**.2 (1983), 91–104. DOI: 10.1007/BF00942715.

[24] C. Wüthrich. The extension of the J-integral concept to fatigue cracks. *International Journal of Fracture* **20**.2 (1982), R35–R37. DOI: 10.1007/BF01141264.

[25] B. Alfredsson and M. Olsson. Initiation and growth of standing contact fatigue cracks. *Engineering Fracture Mechanics* **65**.1 (2000), 89–106. DOI: 10.1016/S0013-7944(99)00108-3.

[26] R. Döring, J. Hoffmeyer, T. Seeger, and M. Vormwald. Short fatigue crack growth under nonproportional multiaxial elastic-plastic strains. *International Journal of Fatigue* **28**.9 (2006), 972–982. DOI: 10.1016/j.ijfatigue.2005.08.012.

[27] T. Hoshide and D. Socie. Mechanics of mixed mode small fatigue crack growth. *Engineering Fracture Mechanics* **26**.6 (1987), 841–850. DOI: 10.1016/0013-7944(87)90033-6.

[28] J. Hutchinson. Singular behaviour at the end of a tensile crack in a hardening material. *Journal of the Mechanics and Physics of Solids* **16**.1 (1968), 13–31. DOI: 10.1016/0022-5096(68)90014-8.

[29] W.-R. Chen and L. Keer. Fatigue crack growth in mixed mode loading. *Journal of engineering materials and technology* **113**.2 (1991), 222–227. DOI: 10.1115/1.2903396.

[30] Y. Hos and M. Vormwald. Experimental study of crack growth under non-proportional loading along with first modeling attempts. *International Journal of Fatigue* **92** (2016), 426–433. DOI: 10.1016/j.ijfatigue.2016.03.036.

[31] J. Tillberg, F. Larsson, and K. Runesson. On the role of material dissipation for the crack-driving force. *International Journal of Plasticity* **26**.7 (2010), 992–1012. DOI: 10.1016/j.ijplas.2009.12.001.

[32] P. Steinmann. Application of material forces to hyperelastostatic fracture mechanics. I. Continuum mechanical setting. *International Journal of Solids and Structures* **37**.48 (2000), 7371–7391. DOI: 10.1016/S0020-7683(00)00203-1.

[33] B. Näser, M. Kaliske, and R. Müller. Material forces for inelastic models at large strains: application to fracture mechanics. *Computational Mechanics* **40**.6 (2007), 1005–1013. DOI: 10.1007/s00466-007-0159-9.

[34] J. Brouzoulis and M. Ekh. Crack propagation in rails under rolling contact fatigue loading conditions based on material forces. *International Journal of Fatigue* **45** (2012), 98–105. DOI: 10.1016/j.ijfatigue.2012.06.002.

[35] P. Zerres and M. Vormwald. Review of fatigue crack growth under non-proportional mixed-mode loading. *International Journal of Fatigue* **58** (2014). Fatigue Crack Paths 2012, 75–83. DOI: 10.1016/j.ijfatigue.2013.04.001.

[36] M. E. Gurtin. A gradient theory of single-crystal viscoplasticity that accounts for geometrically necessary dislocations. *Journal of the Mechanics and Physics of Solids* **50**.1 (2002), 5–32.

[37] M. Fonte and M. de Freitas. Marine main engine crankshaft failure analysis: A case study. *Engineering Failure Analysis* **16**.6 (2009). Papers presented at the Third International Conference on Engineering Failure Analysis (Sitges, Spain, 13–16 July 2008) Part II, 1940–1947. DOI: 10.1016/j.engfailanal.2008.10.013.

[38] M. Fonte, L. Reis, F. Romeiro, B. Li, and M. Freitas. The effect of steady torsion on fatigue crack growth in shafts. *International Journal of Fatigue* **28**.5 (2006). Selected papers from the 7th International Conference on Biaxial/Multiaxial Fatigue and Fracture (ICBMFF), 609–617. DOI: 10.1016/j.ijfatigue.2005.06.051.

[39] M. de Freitas, L. Reis, M. da Fonte, and B. Li. Effect of steady torsion on fatigue crack initiation and propagation under rotating bending: Multiaxial fatigue and mixed-mode cracking. *Engineering Fracture Mechanics* **78**.5 (2011). Damage Tolerance of Railway Axles, 826–835. DOI: 10.1016/j.engfracmech.2009.12.012.

[40] F. Yang, Z. Kuang, and V. Shlyannikov. Fatigue crack growth for straight-fronted edge crack in a round bar. *International Journal of Fatigue* **28**.4 (2006), 431–437. DOI: 10.1016/j.ijfatigue.2005.07.036.

[41] R. O. Ritchie, F. A. McClintock, H. Nayeb-Hashemi, and M. A. Ritter. Mode III fatigue crack propagation in low alloy steel. *Metallurgical Transactions A* **13**.1 (1982), 101–110. DOI: 10.1007/BF02642420.

[42] E. Tschegg and S. Stanzl. The significance of sliding mode crack closure on mode III fatigue crack growth. *Basic Questions in Fatigue.* **1** (1984), 214–232. DOI: 10.1520/STP23218S.

[43] R. Citarella, M. Lepore, V. Shlyannikov, and R. Yarullin. Fatigue surface crack growth in cylindrical specimen under combined loading. *Engineering Fracture Mechanics* **131** (2014), 439–453. DOI: 10.1016/j.engfracmech.2014.08.017.

[44] F Hourlier and A Pineau. Propagation of fatigue cracks under polymodal loading. *Fatigue and Fracture of Engineering Materials and Structures* **5**.4 (1982), 287–302. DOI: 10.1111/j.1460-2695.1982.tb01237.x.

[45] H. Zhizhong, M. Lihua, and C. Shuzhen. A study of shear fatigue crack mechanisms. *Fatigue and Fracture of Engineering Materials and Structures* **15**.6 (1992), 563–572. DOI: 10.1111/j.1460-2695.1992.tb01295.x.

[46] Abaqus. Version 6.13 Documentation (Abaqus). *Abaqus user's guide* (2013).

[47] K. Tanaka. Mechanisms and mechanics of short fatigue crack propagation. *JSME International Journal* **30**.259 (1987), 1–13. DOI: 10.1299/jsme1987.30.1.

[48] M. Gladskyi and A. Fatemi. Load sequence effects on fatigue crack growth in notched tubular specimens subjected to axial and torsion loadings. *Theoretical and Applied Fracture Mechanics* **69** (2014), 63–70. DOI: 10.1016/j.tafmec.2013.12.001.

[49] F. Erdogan and G. C. Sih. On the Crack Extension in Plates Under Plane Loading and Transverse Shear. *Journal of Basic Engineering* **85**.4 (1963), 519. DOI: 10.1115/1.3656897.

[50] G. C. Sih. Strain-energy-density factor applied to mixed mode crack problems. *International Journal of Fracture* **10**.3 (1974), 305–321. DOI: 10.1007/BF00035493. eprint: I248-1974-003.

[51] J. Qian and A. Fatemi. Fatigue crack growth under mixed-mode I and II loading. *Fatigue and Fracture of Engineering Materials and Structures* **8**.4 (1985), 315–325. DOI: 10.1111/j.1460-2695.1996.tb00950.x.

[52] A. M. A. Mageed and R. K. Pandey. Mixed mode crack growth under static and cyclic loading in Al-alloy sheets. *Engineering Fracture Mechanics* **40**.2 (1991), 371–385. DOI: 10.1016/0013-7944(91)90271-2.

[53] P. Dahlin and M. Olsson. The effect of plasticity on incipient mixed-mode fatigue crack growth. *Fatigue and Fracture of Engineering Materials and Structures* **26**.7 (2003), 577–588. DOI: 10.1046/j.1460-2695.2003.00622.x.

[54] N. Simha, F. Fischer, G. Shan, C. Chen, and O. Kolednik. J-integral and crack driving force in elastic–plastic materials. *Journal of the Mechanics and Physics of Solids* **56**.9 (2008), 2876–2895. DOI: 10.1016/j.jmps.2008.04.003.

[55] F. Hourlier, H. D'Hondt, M. Truchon, and A. Pineau. "Fatigue crack path behavior under polymodal fatigue." *ASTM Special Technical Publication*. 1985, pp. 228–248. DOI: 10.1520/STP36226S.

[56] P. E. Bold, M. W. Brown, and R. J. Allen. A review of fatigue crack growth in steels under mixed mode I and II loading. *Fatigue and Fracture of Engineering Materials and Structures* **15**.10 (1992), 965–977. DOI: 10.1111/j.1460-2695.1992.tb00025.x.

[57] A. Otsuka, H. Sugawara, and M. Shomura. A test method for mode II fatigue crack growth relating to a model for rolling contact fatigue. *Fatigue and Fracture of Engineering Materials and Structures* **19**.10 (1996), 1265–1275. DOI: 10.1111/j.1460-2695.1996.tb00949.x.

[58] P. Bold, M. Brown, and R. Allen. Shear mode crack growth and rolling contact fatigue. *Wear* **144**.1 (1991), 307–317. DOI: 10.1016/0043-1648(91)90022-M.

[59] J. W. Ringsberg and A. Bergkvist. On propagation of short rolling contact fatigue cracks. *Fatigue and Fracture of Engineering Materials and Structures* **26**.10 (2003), 969–983.

[60] V Bordi, C. Dorier, and B Villechaise. A Finite Element Analysis of Crack Initiation and Propagation in a Notched Disk Submitted to Rolling Contact Fatigue. *Journal of Tribology* **120**.3 (1998), 436. DOI: 10.1115/1.2834568.

[61] P. Bold. "Multiaxial fatigue crack growth in rail steel." PhD thesis. University of Sheffield, 1990.

[62] D Hannes and B Alfredsson. Rolling contact fatigue crack path prediction by the asperity point load mechanism. *Engineering Fracture Mechanics* **78**.17 (2011), 2848–2869. DOI: 10.1016/j.engfracmech.2011.07.012.

[63] K. Runesson, F. Larsson, and P. Steinmann. On energetic changes due to configurational motion of standard continua. *International Journal of Solids and Structures* **46**.6 (2009), 1464–1475.

[64] A. Otsuka, K. Mori, and T. Miyata. The condition of fatigue crack growth in mixed mode condition. *Engineering Fracture Mechanics* **7**.3 (1975), 429–439. DOI: 10.1016/0013-7944(75)90043-0.

[65] H. Vehoff and P. Neumann. In situ sem experiments concerning the mechanism of ductile crack growth. *Acta Metallurgica* **27**.5 (1979), 915–920. DOI: 10.1016/0001-6160(79)90126-3.

[66] A. Otsuka, K. Tohgo, T. Kiba, and S. Yamada. "Mode II fatigue crack growth characteristics and mechanism in aluminum alloy 7N01-T4 weldments under mode II loading". *Fracture 84*. Ed. by S. Valluri, D. Taplin, P. R. Rao, J. Knott, and R. Dubey. Pergamon, 1984, pp. 1671–1678. DOI: 10.1016/B978-1-4832-8440-8.50159-9.

[67] Z. Ding, Z. Gao, C. Ma, and X. Wang. Modeling of I + II mixed mode crack initiation and growth from the notch. *Theoretical and Applied Fracture Mechanics* **84** (2016), 129–139. DOI: 10.1016/j.tafmec.2016.03.011.

[68] A Rohatgi. *WebPlotDigitizer-web based plot digitizer version 3.11*. 2017.

[69] Y. Jiang and H. Sehitoglu. Modeling of Cyclic Ratchetting Plasticity, Part I: Development of Constitutive Relations. *Journal of Applied Mechanics* **63**.3 (1996), 720. DOI: 10.1115/1.2823355.

[70] D. I. Fletcher and J. H. Beynon. The effect of intermittent lubrication on the fatigue life of pearlitic rail steel in rolling-sliding contact. *Proceedings of the Institution of Mechanical Engineers, Part F: Journal of Rail and Rapid Transit* **214**.3 (2000), 145–158. DOI: 10.1243/0954409001531270.

[71] D. Systemes. *DraftSight: Professional-grade, free* CAD software*. 2012.

[72] D. Floros. *abaqusMesh2Matlab: Program for extracting FE-mesh data, version 1.1*. 2018.

[73] J. Chaboche. On some modifications of kinematic hardening to improve the description of ratchetting effects. *International Journal of Plasticity* **7**.7 (1991), 661–678. DOI: 10.1016/0749-6419(91)90050-9.

[74] M. Ekh, A. Johansson, H. Thorberntsson, and B. L. Josefson. Models for cyclic ratchetting plasticity–integration and calibration. *Journal of Engineering Materials and Technology* **122**.1 (2000), 49–55. DOI: 10.1115/1.482764.